Analyzing glacier retreat and mass balances using aerial and UAV photogrammetry in the Ötztal Alps, Austria.

Joschka Geissler[1,4], Christoph Mayer[2], Juilson Jubanski[1], Ulrich Münzer[3] & Florian Siegert[1]

[1]3D Reality Maps GmbH, Dingolfinger Str. 9, Munich, 81673, Germany
5   [2]Bavarian Academy of Science, Geodesy and Glaciology, Alfons-Goppel Str. 11, Munich, 80539, Germany
[3]Ludwig-Maximilians-University, Department of Earth and Environmental Sciences, Section Geology (remote sensing), Luisenstr. 37, 80333 Munich, Germany
[4]Faculty of Environment and Natural Sciences, Albert-Ludwigs University Freiburg, Friedrichstr.39, 79098 Freiburg, Germany

10   *Correspondence to*: Florian Siegert (Siegert@realitymaps.de)

Abstract. We use high-resolution aerial photogrammetry within the AlpSenseBench project to investigate glacier retreat in great spatial and temporal detail in the Ötztal Alps, a heavily glacierized area in Austria. Long-term in-situ glaciological observations are available for this region as well as a multitemporal time series of digital aerial images with a spatial resolution of 0.2 m acquired over a period of 9 years. Digital surface models (DSMs) are

15   generated for the years 2009, 2015, and 2018. Using these, glacier retreat, extent, and surface elevation changes of all 23 glaciers in the region, including the Vernagtferner, are analyzed. Due to different acquisition dates of the large-scale photogrammetric surveys and the glaciological data, a correction is successfully applied using a designated unmanned aerial vehicle (UAV) survey across a major part of the Vernagtferner. The correction allows a comparison of the mass balances from geodetic and glaciological techniques – both quantitatively and spatially.

20   The results show a clear increase in glacier mass loss for all glaciers in the region, including the Vernagtferner, over the last decade. Local deviations and processes, such as the influence of debris cover, crevasses, and ice dynamics on the mass balance of the Vernagtferner are quantified. Since those local processes are not captured with the glaciologieglaciological method, they underline the benefits of complementary geodetic surveying. The availability of high-resolution multi-temporal digital aerial imagery for most of the glaciers in the Alps provides

25   opportunities for a more comprehensive and detailed analysis of climate change induced glacier retreat. and mass loss.

1   Introduction

The impacts of climate change are widespread and clearly visible in the Alps (Rogora et al., 2018) but particularly evident in the dwindling glacier resources (Beniston et al., 2018; Sommer et al., 2020; Zekollari et al., 2019). Over the past 100 years, the temperature in the European Alps, hereafter referred to as the Alps, has increased almost twice as fast compared to the global average, resulting in nearly 2 °C higher mean air temperatures (Auer et al., 2007; Marty and Meister, 2012). By the end of this century, mean air temperatures are expected to rise further by several degrees Celsius (Gobiet et al., 2014; Hanzer et al., 2018). Due to this ongoing climate evolution, alpine glaciers may lose half of their volume by 2050 compared to 2017 (Zekollari et al., 2019). The response of glaciers to climatic variations is related to the glacier mass balance that can be measured, among others, directly, using the glaciological method, or indirectly, using the geodetic method. For the latter, the volume change of a glacier is determined by integrating the elevation change between two surveys across the entire glacier surface. Volume change is then converted to mass change by incorporating a density assumption of the affected volume. For retrieving geodetic mass balance data, different remote sensing methods exist, varying in the platform (e.g. satellite, airplane, UAV) and sensor (e.g. Laser Scanner, Optic Camera, Radar) used. Their specific benefits and limitations are analyzed and discussed in different studies (Baltsavias et al., 2001; Bamber and Rivera, 2007; Kääb, 2005; Kargel et al., 2013; Pellikka and Rees, 2010).

Glaciological mass balances date back far into the last century and our knowledge of long-term glacier evolution is based on these data sets (Mayer et al., 2013a; WGMS, 2020). However, glaciological mass balances are limited to a few glaciers only, due to the large effort involved in the field work. Existing historic aerial imagery can also provide valuable information on long term glacier evolution and, depending on the imagery, allow a retrospective determination of geodetic glacier mass balances for a considerable number of glaciers and thus greatly complement glaciological data (Belart et al., 2019; Jaenicke et al., 2006; Magnússon et al., 2016; Mayer et al., 2017). Different studies demonstrate the potential of spatiotemporal change analysis of alpine glaciers using photogrammetric data (Fugazza et al., 2018; Gudmundsson and Bauder, 1999; Legat et al., 2016; Rossini et al., 2018) and comparing their results to glaciological mass balances (Baltsavias et al., 2001; Klug et al., 2018). Comparing geodetic and glaciological mass balances generally has the potential to reveal systematic errors and regions of anomalous mass balance conditions (Fischer, 2011). However, when comparing these methods one needs to account for different error sources such as differences in survey dates, errors related to the density assumption, ice dynamics, internal and basal melt and other systematic or random error sources (Pellikka and Rees, 2010; Zemp et al., 2013).

Zemp et al. (2013) provides a framework to perform homogenization, error assessment and calibration of the geodetic and glaciological data sets that is often used in the scientific community (Andreassen et al., 2016; Klug et al., 2018). Building on this framework, considering the required additional data is available, we see further potential (i) regarding the involved density assumption as well as (ii) for extrapolating geodetic mass balances to full mass balance years. These small improvements increase the detail of our geodetic mass balance and thus allow a more in-depth comparison of the geodetic and glaciological mass balances and will be presented within this study.

Regarding volume to mass conversion (i), the simple density assumption provided by Huss (2013) is frequently used to derive overall geodetic mass balances (Andreassen et al., 2016; Belart et al., 2019). However, this assumption is only valid for periods longer than three to five years, medium to high volume change and stable

mass balance gradients (Huss, 2013, Zemp et al, 2013). These strong limitations are often overcome by using firn densification models (~~e.g.~~ Reeh, 2008~~),~~), existing field datasets (Huss et al., 2009) or pixel-based classifications of snow, firn and ice and assigning a density to each class (Pelto et al., 2019). However, those methods require

70   extensive field measurements and computational effort. We present an easy applicable and transferrable approach, incorporating the equilibrium line altitude (ELA) of a glacier to generate an altitude-related density assumption with a linear transition around the ELA from firn to ice density. The required ELA can be retrieved from satellite imagery (Rabatel et al., 2005) or historic photographs (Vargo et al., 2017).

For the comparison of geodetic and ~~glaciologic~~glaciological data, extrapolating the mass balances to full mass

75   balance years (30th September) (ii) is required, since survey dates usually differ. Such corrections can for instance be applied by using a simple degree-day model (Belart et al., 2019) or field measurements (Fischer et al., 2011). These methods, however, are either not suitable for retrospective corrections where no field data was collected or do not account for the spatially distributed, glacier specific accumulation and ablation patterns of each glacier (Huss et al., 2009). We present a workflow for using an UAV survey with 5 cm spatial resolution, in combination

80   with a simple degree-day model to correct differences in survey dates between geodetic and ~~glaciologic~~glaciological data. This robust approach allows a more detailed analysis of the ice dynamics and the remaining systematic differences between the geodetic and ~~glaciologic~~glaciological mass balances.

This study is focused on a study site within the Ötztal Alps, Austria. Airborne photogrammetric datasets covering 23 glaciers are provided by the Austrian Bundesamt für Eich- und Vermessungswesen (BEV) and 3D RealityMaps

85   GmbH for 2009, 2015 and 2018, thus covering a period of 9 years. One of the surveyed glaciers is the Vernagtferner, a reference glacier in the World Glacier Monitoring Service (WGMS) system. ~~Glaciologic~~Glaciological mass-balances have been determined here using the glaciological method since 1965, while a series of historical maps back to 1889 demonstrates the long-term glacier evolution over more than a century (Escher-Vetter et al., 2009).

90   Within this study, we describe the full photogrammetric workflow applied to our aerial imagery. After the coregistration of the resulting DEMs, volume changes and general glacier retreat is analyzed for all 23 glaciers. A more detailed analysis is conducted for the Vernagtferner, where our altitude-related density assumption and the UAV-based correction of survey dates allows a spatial and quantitative comparison of the geodetic with the ~~glaciologic~~glaciological mass balances.

95   **2   Study Area**

The Ötztal Alps are located in the central-eastern Alps and represent one of Austria's most extensive glacierized regions, covering a range in altitude between 1700 to 3768 meters above sea level (m.a.s.l.) and more than 250 km² (Fig. 1). It combines the upper regions of the drainage basins of Rofental, Pitztal, and Kaunertal. The location in the inner part of the Alps leads to relatively low precipitation amounts (Fliri, 1975, 186-197), which for example,

100   reach mean values of 660 mm yr^{-1} at the valley station Vent in 1969-2006 (Abermann et al., 2009).

For some of the 23 glaciers within the study site, ~~glaciologic~~glaciological mass balance measurements exist. One of the longest series of measurements can be found at the Vernagtferner, where regular monitoring by the Bavarian Academy of Sciences and Humanities (BAdW) began in 1965 (Escher-Vetter et al., 2009). This glacier is characterized by several sub-basins, which were connected to a single glacier tongue in former times. In 2018, the

105   glacier covered almost 7 km² within an altitude range between 2860 m.a.s.l. and 3570 m.a.s.l.. The mass balance

3

is determined by the glaciological method, using measurements at ablation stakes, manual and geophysical depth soundings, and retrieving information from snow and firn pits. The annual and winter mass balances are determined independently of each other by measurements on the fixed dates of 1st May and 30th September, the dates of the glaciological balance year (Cogley, 2010; Cogley et al., 2011). Besides, there is a long history of

110   geodetic mapping at the Vernagtferner dating back to 1889 (Mayer et al., 2013a).
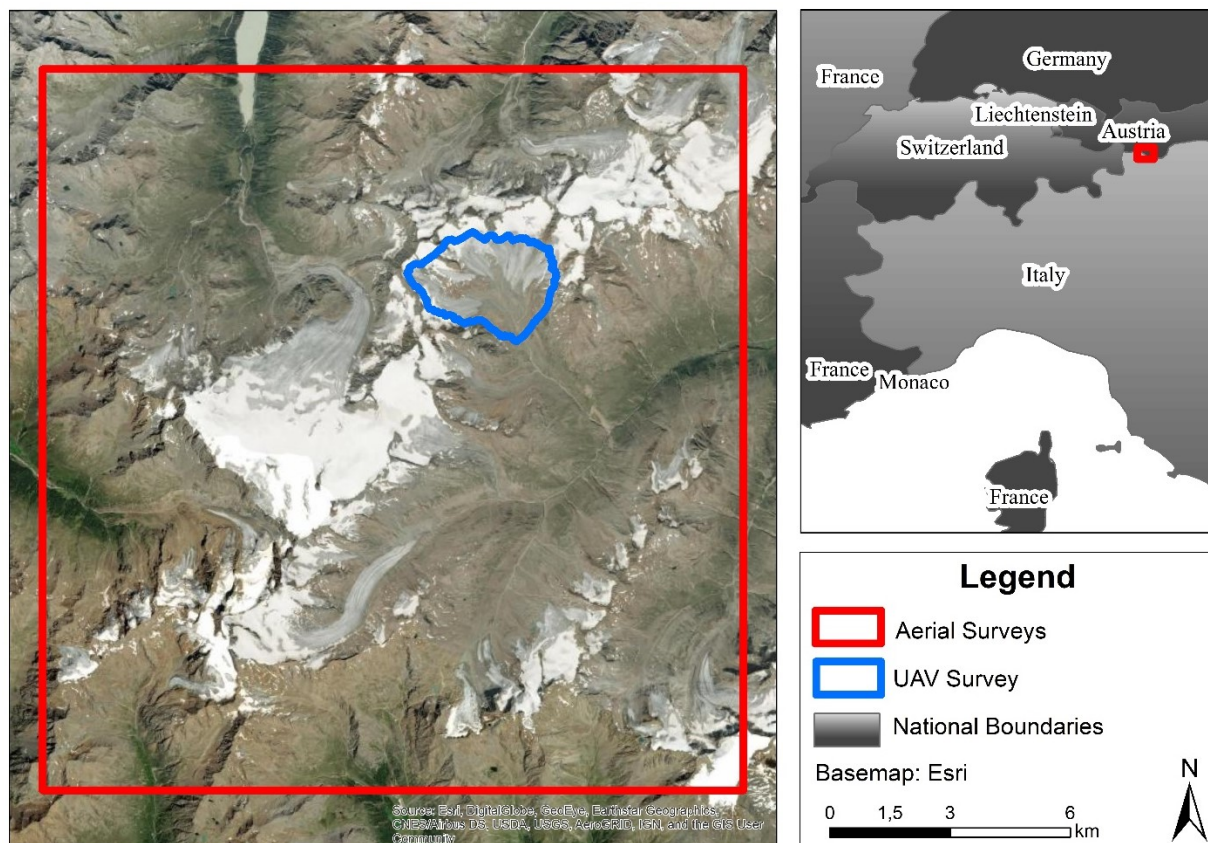
Figure 1: Study site in the Ötztal Alps; Red: area covered by aerial surveys; Blue: area of the Vernagtferner covered by the UAV Survey; Image source: ESRI (2020)

3   Data Acquisition

115   **3.1   Photogrammetric data**

In Austria, cadastral aerial surveys are conducted by the BEV with a nominal resolution of 0.2 m. We use a BEV survey from 2015 as a basis for our investigations. Besides, surveys performed by 3D RealityMaps in 2009 and 2018 with the same or higher ground resolution are investigated. Table 1 shows the most relevant information on the conducted air surveys.

120   In addition to the airplane-based surveys, a smaller test site was covered by an UAV flight to retrieve high-resolution data at another acquisition date closer to the maximum of ablation in 2018 (Table 1). The processed area covers 6 km² containing most of the Vernagtferner, including all glacier tongues. The glacier was almost snow-free at the time of the acquisition, which provides optimal processing conditions.

125

Table 1: Overview of the aerial data acquisitions

Date	Platform	Area [km²]	Overlap (forward:~~lateral~~side) [%]	Resolution [cm]	Images [Count]	Image type	Camera
09.09.2009	Airplane	257	80:40	20	381	TIF RGB 8bit	UltraCam XP
03.08.2015	Airplane	330	80:50	20	572	TIF RGBI 16bit	UltraCam XP
21.09.2018	Airplane	260	80:60	20	428	TIF RGBI 16bit	UltraCam Eagle Mark 2
21.08.2018	UAV	6	80:80	5	1992	JPEG RGB 8bit	UMC-R10C

3.2 Glaciological mass balance data

Glaciological mass balance data is gathered as stake readings from ablation stakes for estimating the ice melt
across the glacier. Snow depth and last season firn deposits are determined from mechanical depth soundings with
metal probes, which are then combined with density information from snow and firn pits to calculate the water
equivalent of the remaining snow and firn cover. While stake readings only require two length measurements per
stake with an uncertainty of typically about 1 cm, more significant errors are included in the direct accumulation
measurements due to uncertainties in the sample volume (about 5%) and the determination of density by using
spring scales (about 4%). Therefore water equivalent accuracy is about 6% (Zemp et al., 2013). The typical number
of stakes used for the annual mass balance measurements at the Vernagtferner is about 35, while 4-5 accumulation
measurements are collected at the end of the glaciological year, 30th September.

Glacier boundaries for delineating the spatial mass balance distribution are derived from aerial surveys repeated
roughly every decade, updated in the ablation region by annual GNSS (Global Navigation System Services)
measurements of the glacier tongue geometry. The spatial error of these measurements is usually better than 1 m.
The information from the stake readings, the depth soundings, the snow and firn pits, and the location of the
equilibrium line are combined to interpolate the spatial distribution of the glacier mass balance into a raster file.
Due to the sparse information in the accumulation region, it is necessary to manually correct the interpolation
results in this region with the knowledge of the long-term accumulation patterns, which are rather persistent. Errors
introduced by uncertainties in the accumulation region, however, are relatively small, especially during the recent
decade where the accumulation area ratio (AAR) is usually well below 30 %. While ablation varies between 0 and
up to 4.5 m w.e. a^{-1} in the ablation area, accumulation only varies between 0 and about 0.3-0.4 m w.e. a^{-1} in the
accumulation area. Within this study, we assumed the error of the interpolated ~~glaciologie~~glaciological raster to
be 0.1 m. w.e. a^{-1}, which is in accordance with Zemp et al. (2013). It must be noted that this relatively large error
within the accumulation area will only affect the final mass balance by less than 2 %.

The ELA is derived by comparing oblique terrestrial photographs of the transient snow line and firn extent with
optical remote sensing information close to the field measurements date. The derived ELA has a horizontal location
accuracy of about 10 m.

4   Methods

4.1   Photogrammetric workflow

To determine geodetic glacier mass balances from aerial and UAV images, we used a workflow consisting of two main modules: the data processing (Sect. 4.1.1) and the vertical change analysis (Sect. 4.1.2; Fig. 3). The main goal of the data processing module was the reconstruction from raw imagery data into 3D point clouds. Digital Surface Models (DSM) and ~~True Orthophoto Mosaics (TOM)~~orthophotos were then derived from these point clouds. Finally, DSM differences were computed. Within the vertical change analysis module, geodetic glacier mass balances were computed from the DSM differences.
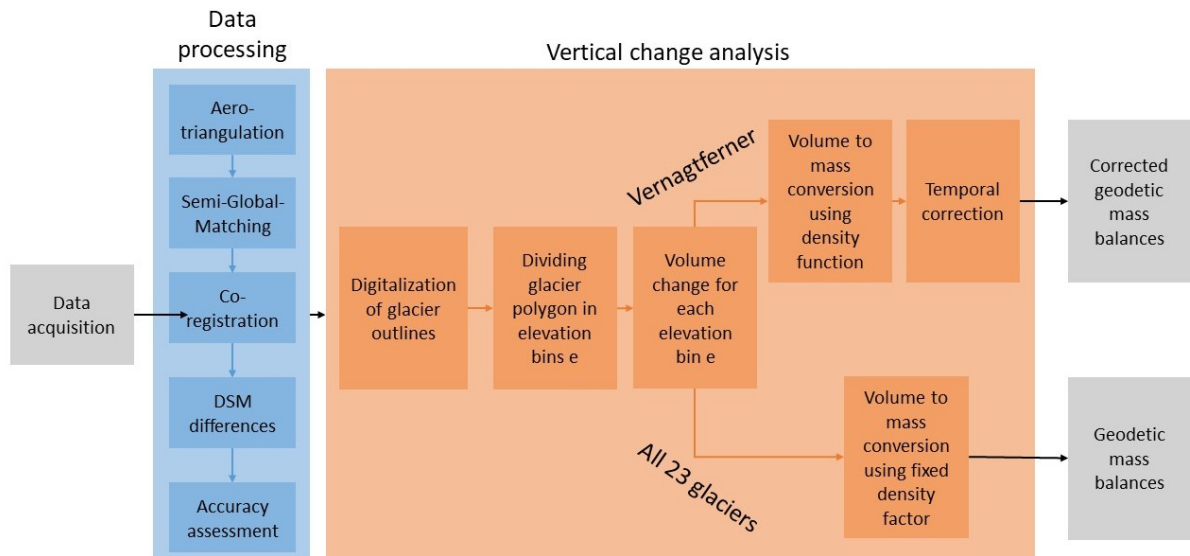
Figure 2: Full workflow; Blue: From raw images to DSM differences; Orange: From DSM differences to overall and altitudinal mass balances

4.1.1   Data processing

The first step in data processing was the aerotriangulation, which consists of the orientation of the aerial imagery to the real terrain. Modern photogrammetric survey systems deliver highly accurate positions using GNSS and orientation (IMU, inertial measurement unit) information for each image, which were also included in the aerotriangulation for the georeferencing. Finally, at least 20 tie points were manually identified for each image block to enhance the orientation accuracy. For the large format imagery, the aerotriangulation was performed using the software *Match-AT* by Trimble. For the UAV imagery, the software *Metashape Professional* from Agisoft was used.

The second stage of data processing was the generation of point clouds through three-dimensional reconstruction. For this purpose, the state-of-the-art Semi-global-matching algorithm (Heipke, 2017; Hirschmüller, 2019) was used. This algorithm was implemented within the software *SURE* (nFrames), which generates DSM and ~~TOM~~orthophotos from the point clouds. The horizontal shift of the derived ~~TOM~~orthophotos and ~~DSM~~DSMs was computed based on ground control points from the BEV and lies between 10 and 20 cm depending on the acquisition year and thus within the ground resolution of the images. Due to these excellent values, only a vertical coregistration of the DSM differences was applied. Therefore, existing systematic height shifts between all DSMs

6

were derived using 50 stable points (e.g., solid rock) outside the glaciers. 21 stable points were used for the UAV-survey. The 2015 DSM was chosen as the reference because it was derived from the official Austrian cadastral survey and is referenced to the Austrian national survey system. Based on this mean vertical shift over stable ground, all DSMs except for the reference DSM were adjusted in height relative to the reference DSM of 2015. Subsequently, the DSM differences 9/2018–8/2015, 8/2015–9/2009, 9/2018–9/2009, and 9/2018–8/2018 were computed ~~and named after their acquisition dates.~~.

4.1.2 Vertical change analysis

The goal of the vertical change analysis (Fig. 2, orange part) was to quantify elevation changes Δh_t within our study area from the DSM differences of different time periods t. By integrating Δh_t over a specific area S_t, volume change ΔV was determined by the following equation, where r is the pixel size (Fischer, 2011; Zemp et al., 2013):

$$\Delta V_t = r^2 * \int_0^{S_t} \Delta h_t \tag{1}$$

To derive overall geodetic glacier mass balances $B_{geod,t}$, ΔV_t was determined with S_t being the area at the beginning of the respective period t (Fischer, 2011). S_t was digitized visually using ~~TOM~~orthophotos at a scale of 1:~~2.000~~2000. For the following volume to mass conversion (Zemp et al., 2013), we used the density assumption proposed by Huss (2013) ($\bar{\rho}$= 850 kg m^{-3} ± 60 kg m^{-3}) for all glaciers.

$$B_{geod,t} = \frac{\Delta V}{\bar{S}} * \frac{\bar{\rho}}{\rho_{water}} \quad \text{with} \quad \bar{S} = \frac{S_{t=begin} + S_{t=end}}{2} \tag{2}$$

To allow a detailed analysis of the altitudinal dependencies of the glacier mass balances, the glacier area was divided into 10 m elevation bins e. For each bin, the geodetic mass balance $B_{geod,e,t}$ was derived with the same equations (see Eq. 1, 2 and Zemp et al. (2013)).

In contrast to most of the glaciers within our study area, the ELA (Sect. 3.2.) of the Vernagtferner is known and lies at 3217 m.a.s.l. for the period 2009-2015, 3278 m.a.s.l. for the period 2015–2018 and, averaged over the entire study period, at 3237 m.a.s.l. for 2009-2018. Thus, we were able to use an altitude-related density function $\bar{\rho} = f_{t,d}(e)$ for converting surface changes to mass relative to the altitude of the ELA for the Vernagtferner (Figure 2). This density function $f_{t,d}(e)$ [kg m^{-3}] represents the gradual change from ice density (900 kg m^{-3}) in the ablation region to firn density (550 kg m^{-3} (Cogley et al., 2011)) in the accumulation region with elevation e, by using a linear transition zone of ±50 m around the ELA of the respective period t:

$$f_{t,d}(e) = \begin{cases} 550 & \text{for e} > \text{ELA} + 50 \text{ m} \\ 725 - 3.5 * (e - ELA_t) & \text{for e between ELA} \pm 50 \text{ m} \\ 900 & \text{for e} < \text{ELA} - 50 \text{ m} \end{cases} \tag{3}$$

4.2 Comparison with glaciological data

To allow a comparison of the geodetic and ~~glaciologic~~glaciological mass balances, both datasets were reanalyzed independently according to the steps 1 to 4 in Zemp et al. (2013): Datasets were homogenized (Sect. 3.2 and 4.1.1.), annual glaciological mass balances were accumulated to the periods 09/2009-09/2015, 09/2015-09/2018, and 09/2009-09/2018, mean annual mass balances of the respective periods (Sect. 3.2. and 4.1.2) as well as systematic and random errors for all geodetic datasets (Sect. 4.3) were derived (Nuth and Kääb, 2011). Because one main objective of this paper was to analyze systematic differences between the two methods, iterative adjustment and calibration of the data (step 5-6, Zemp et al. (2013)) was not performed.

TheWe developed a workflow to account for the remaining temporal differences between the photogrammetric and glaciologic acquisition timesglaciological mass balance data. Correction periods were defined between the survey date of the photogrammetric data and the end of the glaciological year (Table 2addressed using an). An additional photogrammetric DSM difference was derived for one month within the ablation period in 2018 (t=corr) using an UAV survey (Table 1. A). Therefrom, a regression (sigmoid, see Fig. 3) was performed for deriving the altitude dependent surface elevation change $\Delta h_{k,t=corr}$(Table 2() of the respective period t=corr (Table 2). By multiplying $\Delta h_{t=corr}$ with the altitude related density assumption $f_{t,d}(e)$ (Eq. 3) the mass balance $B_{geod,e,t=corr}$ for all elevation bins e and the correction period t=corr (Table 2(08/2018 09/2018)) was derived. Only those altitude levels were considered for the regression, which were at least 40 % covered by the UAV survey. The standard deviation (SD) of the regression is 0.07 m ice (Fig. 3). Above 3180 m.a.s.l., thus, for the accumulation areas, the correction function is not based on any data and is therefore error-prone.
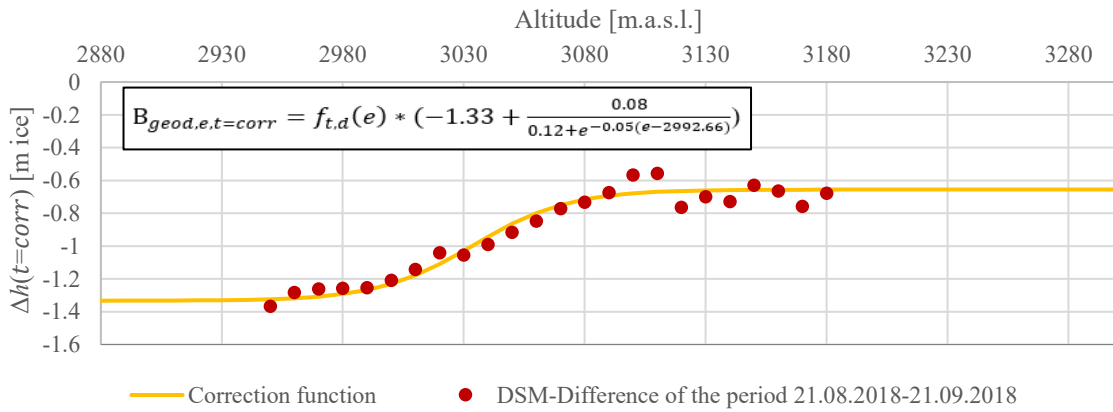

Figure 3: Surface changes in 10 m altitude bins for the correction period (21.08.2018 to 21.09.2018 (red dots); Regression curve (yellow), representing height changes related to the altitude; SD of the regression is 0.07 m ice.

To transfer this information to other timethe correction periods (t=1-3, Table 2,), we used temperature time series measured at a climate station close to the Vernagtferner at 2640 m.a.s.l.. Positive Degree Day Sums (PDD$_{e,t}$) [°C] were computed for all elevation bins e and time periods t (Table 2, the geodetic and glaciologic method needed a correction for (Table 2). For this step). To determine the Degree Day Function (DDF) for all elevation bins, we assumed the vertical lapse rate of the air temperature to be -0.6 °C per 100 meters of altitude. This allowed the Degree Day Function (DDF) to be determined for all elevation bins e (Eq. 4). More information on the DDF method can be found, for instance, in Braithwaite and Zhang (2000) and Hock (2003).

$$\text{DDF}_e = \frac{B_{geod,e,t=corr}}{PDD_{e,t=corr} * d_{t=corr}} \tag{4}$$

The geodetic mass balance for the correction periods $B_{e,t}$ could then be determined for the time periods t of length d_t and in all elevation bins e:

$$B_{geod,e,t} = DDF_e * PDD_{e,t} * d_t \tag{5}$$

Subsequently, the geodetic mass balances of the full study periods $B_{geod,e,\ 09/2009\ -\ 08/2015}$, $B_{geod,e,\ 08/2015\ -\ 09/2018}$, and $B_{geod,e,\ 09/2009\ -\ 09/2018}$ were corrected according to Table 2. and recalculated to an annual basis. In this study, we refer to these temporally corrected geodetic mass balances as annual geodetic mass balances (unit: m. w.e. a^{-1}) and

8

provide the information on the period with full years (e.g. 2009-2018). Uncorrected geodetic mass balances are referred to by year and their respective month (e.g. 09/2009-09/2018).

Table 2 Correction parameters (left) of all correction periods t and the applied corrections to all geodetic mass balances (right).

t	~~Acquisition date photogrammetric data~~Correction periods		d_t [days]	$PDD_{e=2870 \text{ m.a.s.l.}, t}$ [°C]	Applied Corrections
1	09.09.2009	30.09.2009	21	82.45	
2	03.08.2015	30.~~08~~09.2015	~~27~~59	280.76	$B_{geod,e,09-15} = B_{geod,e, 09/2009 - 08/2015} - B_{geod,e,t=1} + B_{geod,e,t=2}$
					$B_{geod,e,15-18} = B_{geod,e, 08/2015 - 09/2018} - B_{geod,e,t=2} + B_{geod,e,t=3}$
3	21.09.2018	30.09.2018	9	46.58	$B_{geod,e,09-18} = B_{geod,e, 09/2009 - 09/2018} - B_{geod,e,t=1} + B_{geod,e,t=3}$
corr	21.08.2018	21.09.2018	31	176.81	

The overall geodetic mass balances $B_{geod, t}$ of the Vernagtferner was then derived from the mass balances of the single elevation bins e and their respective area $S_{e,t}$ (Zemp et al., 2013):

$$B_{geod,t} = \frac{\sum_{e=1}^{E} B_{geod,e,t} * S_{e,t}}{S_t} \tag{6}$$

Finally, accumulated glaciologically derived rasters $B_{glac,t}$ (Sect. 3.2) were subtracted from the adjusted geodetic mass balances $B_{geod,t}$. The resulting Variation Rasters Var_t show the spatial deviations between the two methods, where negative values occur for areas where $B_{glac,t} > B_{geod,t}$ and positive values for the opposite relation.

$$Var_t = B_{geod,t} - B_{glac,t} \tag{7}$$

Using this Variation Raster, we analyzed spatial deviations between both methods that occur due to differences in the individual methods and related errors (e.g., neither including the supra-glacial debris cover or crevassed areas for surface ablation nor dynamic processes within the ~~glaciologic~~glaciological method). Therefore, we digitized the respective areas on the Vernagtferner by using the geodetically derived ~~TOMs~~orthophotos of 2009 and 2018 and computed the mean annual variation (difference between the annual geodetic and the ~~glaciologic~~glaciological mass balances) by using the Variation Raster (Eq. 7) as well as Eq. 1 and 2. By comparing this mean variation with the mean variation of areas within the same elevation bin, we estimated the magnitude of error introduced by neglecting those areas within glaciological mass balances.

4.3 Vertical accuracy assessment

To assess the error distribution within the study area after the coregistration, temporally uncorrected geodetic DSM differences were analyzed following the methodology presented by Nuth and Kääb (2011). Therefore, 1.5 km² of ice-free, stable terrain ~~was analyzed~~, representing a wide range of ~~slope, aspect, and altitude~~topography was digitized manually. The mean shift and the SD within those areas were calculated, and their relation to topography was investigated~~, following Nuth and Kääb (2011).~~. To estimate the error when averaging over extended areas, we followed Rolstad et al. (2009) by assessing the spatial covariance of the elevation differences using semivariograms. Thus, we derived range-values from the semivariograms of all periods and converted those to the confidence intervall of the respective DSM difference. For more detailed information on this method, see Rolstad

9

270   et al. (2009). For the application of the method, we assumed that elevation differences are constant in space, do not contain any large-scale trends, and that there is no significant variation of the variance in space.

Basic error propagation was implemented (Nuth and Kääb, 2011; Zemp et al., 2013) to determine the compound error of DSM differences, density conversion (7 %, Sect. 4.1.2, Huss (2013)), the correction function of the acquisition dates (SD = 0.07 m ice a^{-1}, Sect. 4.2) as well as the error associated to the glaciological interpolation

275   raster (Sect. 3.2) for all presented results. The error within this study is indicated by the 95% confidence interval.

5   Results

5.1   Vertical Change Analysis

5.1.1   Visual assessment

Using the derived glacier outlines, ~~TOMs~~orthophotos, and DSM differences, the first results are obtained by a

280   visual interpretation for the entire study area. In general, glaciers have thinned and reduced in size. For instance, surface height changed at the glacier tongue of the Hintereisferner by up to – 20.4 ± 0.4 m during the nine years from 09/2009 to 09/2018 (Fig. 4). With increasing altitude, the loss of height on the glacier approaches zero. Surface elevation changes around the glacier tongue of the Hintereisferner can be attributed, among others, to local debris movements and an existing dead-ice body (Fig. 4). Analyzing the ~~TOM~~orthophotos of the three surveys

285   reveals that the eastern part of the Hochjochferner lost a considerable area along its lower glacier margin. Especially its main tongue shortened by 826.4 ± 0.2 m between 2009 and 2018 (Fig. 5, white dotted circle). Further visualization of the DSM differences can be assessed at https://og.realitymaps.de/AlpSense/.
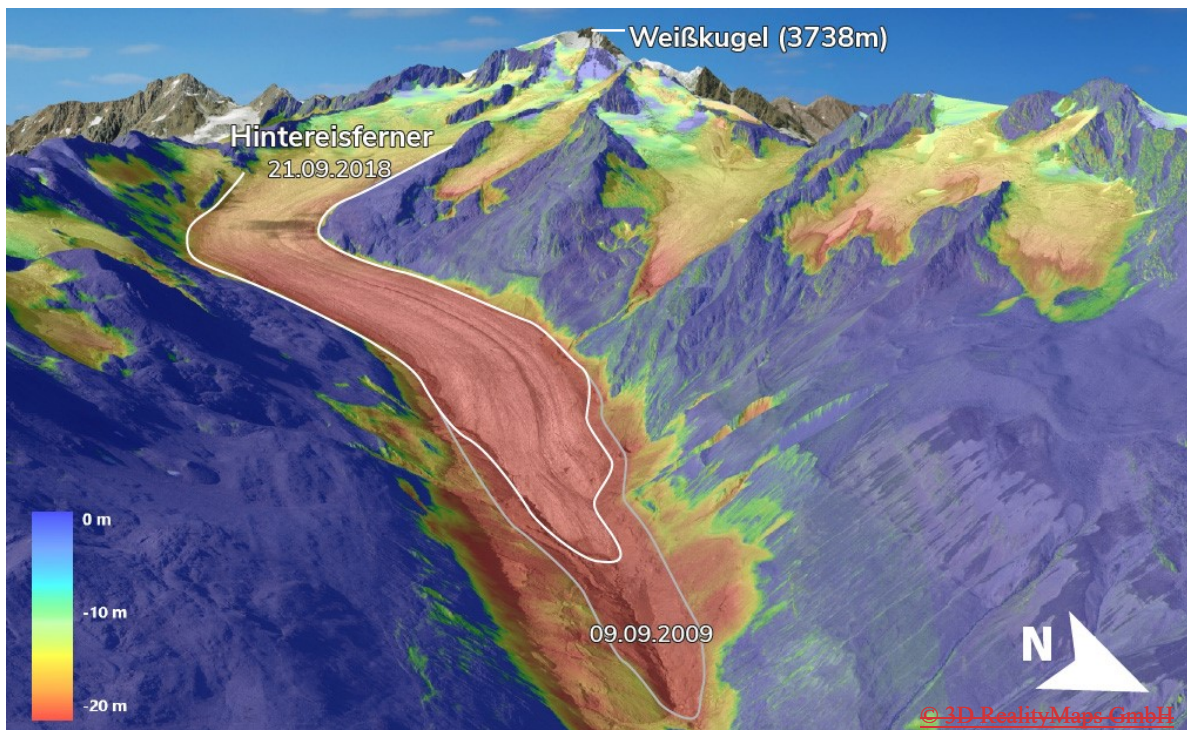

Figure 4: 3D representation of the color-coded height differences in meter (m) between the DSMs of 09/2009 and 09/2018
290   **for Hintereisferner (white outline). Surface elevation loss appears in red, constant elevation appears blue. Ice loss is especially high at altitudes below ~~2.500~~2500 m. The underlying orthophoto was derived from the 2018 aerial survey. Height loss in the south-east of the glacier tongue can likely be attributed to an existing dead-ice body.**
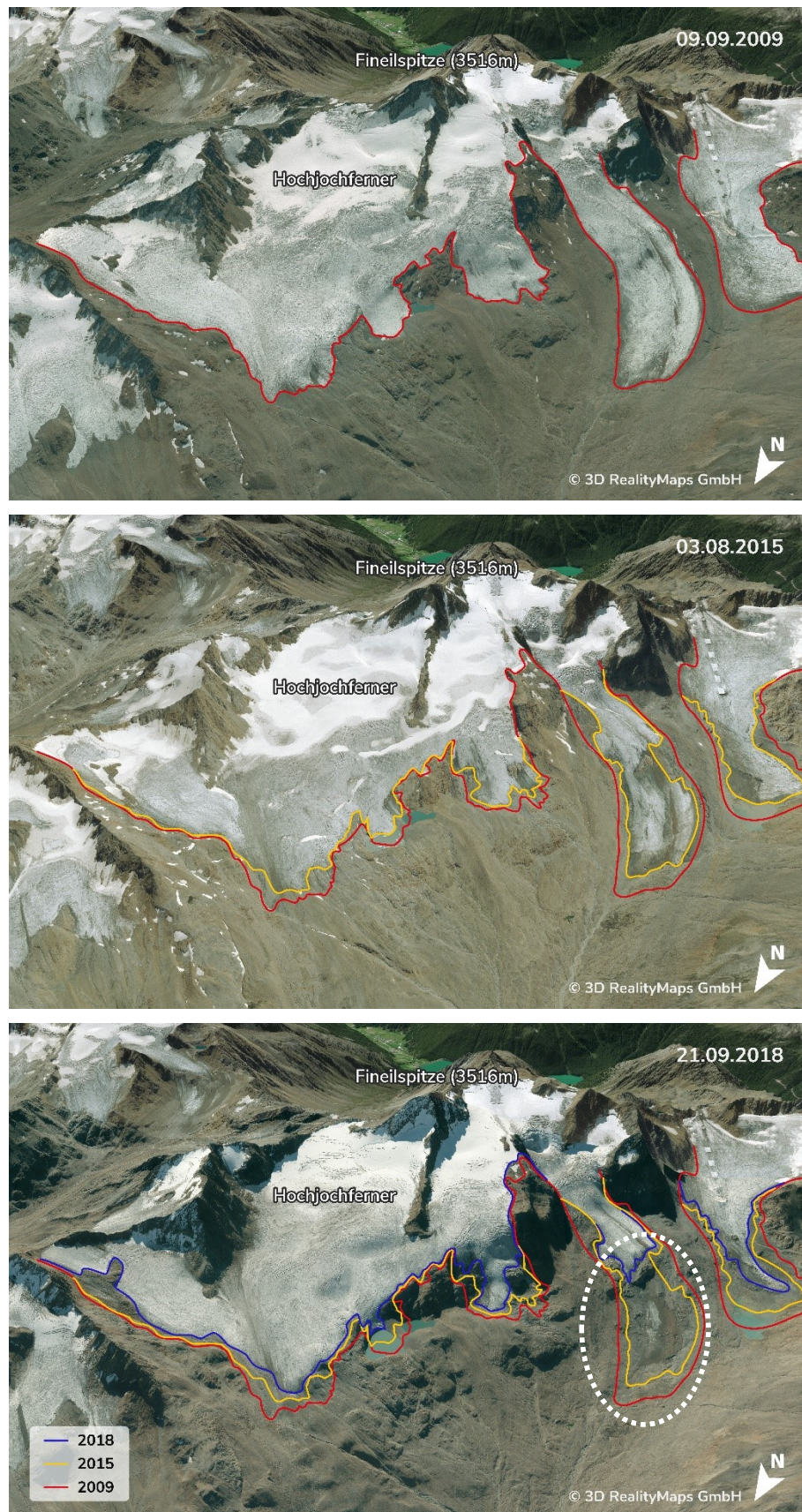
10

Figure 5: 3D visualization of the length change for the Hochjochferner in 2009 (top), 2015 (middle), and 2018 (bottom); Lines indicate glacier extent for the respective years. The second glacier tongue from the right (white dotted circle) lost 826 m in 9 years.

295

5.1.2   Vertical accuracy assessment

The accuracy assessment conducted (Sect. 4.3) allows an estimation of potential error related to the DSM differences and derived products. In general, the mean vertical error of the DSM differences ranges from -0.16 m to 0.10 m with, SD does not exceedingexceed 0.42 m (Fig. 6a).) and errors are generally smaller for the period 08/2015-09/2018. As expected, SD increases with the slope (for both periods (Fig. 6b, e). An apparent increase of the SD can also be found in lower altitudes (< 2600 m.a.s.l., (Fig. 6d, g), most likely due to the increasing influence of vegetation. A relation between aspect and the vertical error was found for the DSM difference 09/2009 – 08/2015 (Fig. 6c), which can be attributed to thea horizontal shift of the DSMsDSM 2009 (Sect. 4.1.1) (Nuth and Kääb, 2011).

Based on the error assessment, the confidence interval for all results within this paper was determined. Therefore, semivariograms were computed for the 1.5 km² bedrock areas for all observation periods, from which the range value (100 m) was conducted and converted to the correlated area value (31416 m²). For more detailed information on this method, see Rolstad et al. (2009).
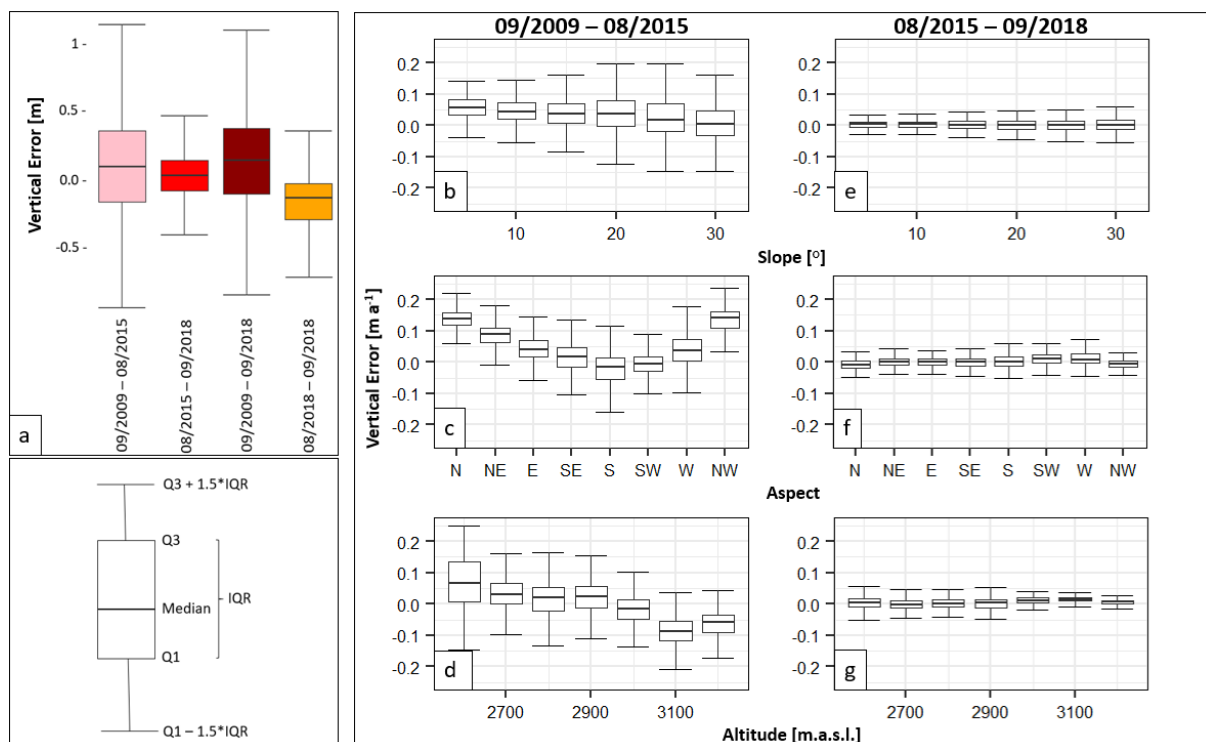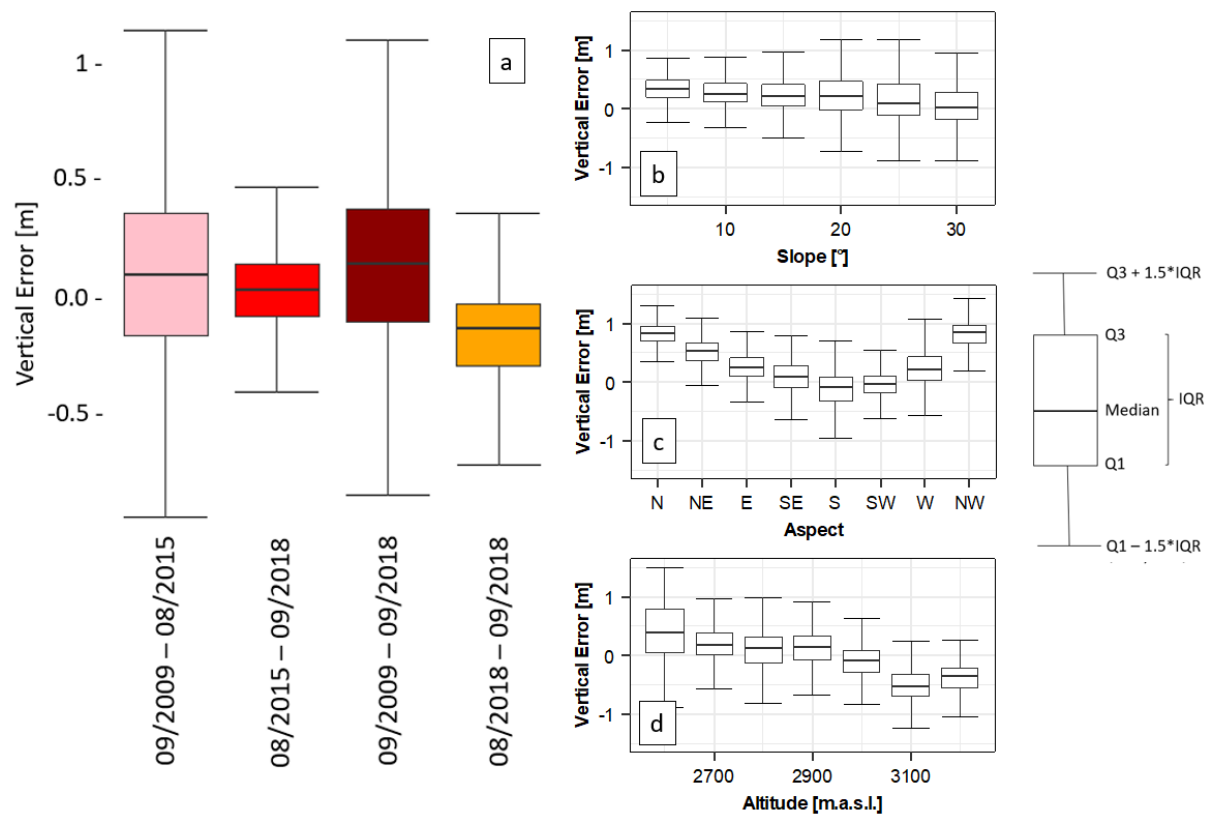
Figure 6: ~~Error assessment~~ Overall vertical error of the DSM differences ~~in general~~ (a~~) and)~~; Annual vertical error for the periods 09/2009-08/2015 (b-d) and 08/2015-09/2018 (e-g) in relation to slope (b,e), aspect (c,f) and altitude (d~~)~~; ~~Boxplots in the right column (b, c, d) have been plotted using the DSM difference 09/2009 - 08/2015~~,g).

13

5.1.3 Mass balances

Volumetric changes $\Delta V_{t,e}$ and height changes $\Delta h(t,e)$ for every elevation bin e were derived for all periods t and
all glaciers, before and (for the Vernagtferner only) after the correction of acquisition dates (Eq. 1 – 2, Fig. 7).
Before and after the temporal correction, the annual height changes per elevation bin show a characteristic shape
with height changes being the most negative at the glacier tongues. The period between 2009 and 2015 generally
shows less negative values than the period 2015 and 2018 in all altitudes for all glaciers (Fig. 7, bottom left) ~~and~~
the Vernagtferner (Fig. 7, top left). ~~After~~Although after the temporal correction, the difference in height change
between the two periods is considerably smaller.

Compared to the height changes, the most negative volume change occurs in higher elevations since it is linked to
the area-height-distribution of a glacier. After correcting for the acquisition dates, based on a regression curve
(Gaussian fit) for the values of the Vernagtferner, between 2009 and 2015, the most negative volume change
of -0.21 ± 0.01 million m³ a⁻¹ occurred at an altitude of 3009-3019 m.a.s.l.. Between 2015 and 2018, the most
negative volume change further decreased to -0.29 ± 0.02 million m³ a⁻¹ at an increased altitude of 3089-3099
m.a.s.l. (Fig. 7, top right). The same trend was found for all glaciers within the study area, although no correction
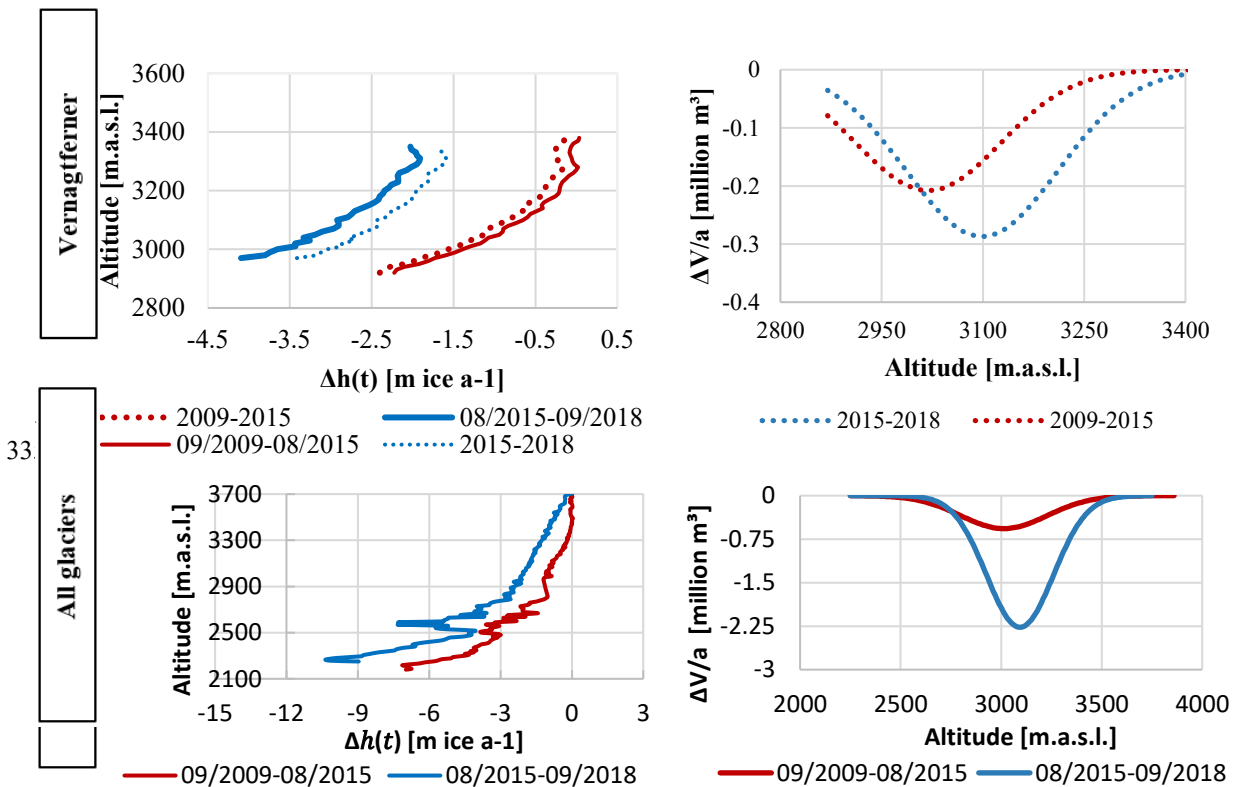was applied to those values (Fig. 7, bottom right).

Figure 7: Top left: Annual height changes $\Delta h(t)$ per altitude for the Vernagtferner, Bottom left: Surface height changes of all glaciers; Right: annual volume changes for the Vernagtferner (top) and all glaciers (bottom); Dotted lines represent the surface or volume changes after the correction of the acquisition dates.

### 5.2 Comparison with glaciological measurements

14

The geodetic and glaciological mass balances of the Vernagtferner were further compared to detect discrepancies in spatial distribution or magnitude between both methods ~~presented~~. As already noted, the overall mass balance for the Vernagtferner is more negative in the period 2015-2018 than in the period 2009-2015. This can be seen in

345 both, the glaciological and the geodetic mass balances (Fig. 8). The uncorrected geodetic mass balance (blue) does not equal the corresponding glaciological mass balance (orange). After the correction of acquisition dates (red), the _annual_ geodetic mass balance has approached the glaciological data. However, the corrected data is still more negative for 2015-2018 and 2009–2018. For the period 2009-2015, corrected geodetic and ~~glaciologic~~glaciological mass balances match.

350
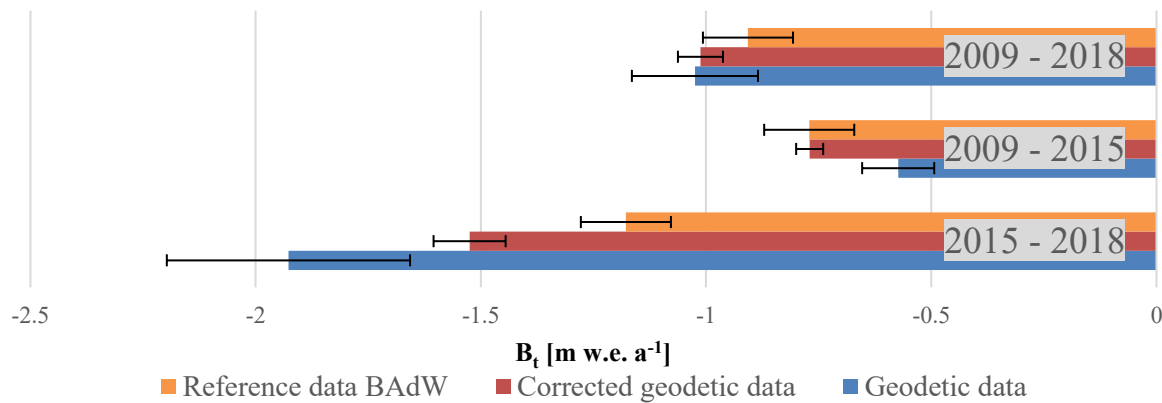
Figure 8: Comparison between geodetic mass balances (blue) and glaciological mass balances (orange) for the investigation periods. Red bars visualize corrected geodetic data.

The spatial differences between both methods were further investigated using the Variation Raster described in sect. 4.2.. It is noticeable that the Variation Raster is more positive (thus $B_{glac,t} < B_{geod,t}$, see Eq. 7) in debris-

355 covered areas compared to its surrounding cells (red in Fig. 10). Since no ablation stakes are located in supra-glacial debris at the Vernagtferner and glaciological mass balances are interpolated from surrounding information on clean ice, the effect of debris is neglected within the ~~glaciologic~~glaciological method. Debris cover above a certain thickness protects the glacier against incoming heat fluxes (Östrem, 1959) and therefore reduces the ablation. With our Variation Raster, we were able to quantify the effect of neglecting debris-covered areas within

360 the glaciological interpolation: For 2018, a total area of 91350 m² (1.5 % of the total area of the Vernagtferner) at a mean altitude of 3040 m.a.s.l. was classified as debris cover. The variation between the geodetic and ~~glaciologic~~glaciological method for those debris-covered areas is ~~5.02 ± 0.89~~56 ± 0.3 m w.e. a^{-1} and thus more positive than the mean variation at the respective altitude $0.38 ± 0.27$ m w.e. a^{-1} (period 2009–2018, see Fig. 9). Considering the difference of those values, the overall ~~glaciologic~~glaciological mass balance of 2009-2018 would

365 be 0.~~07~~17 m w.e. a^{-1} (~~7.7~~2 %) less negative if debris-covered areas were considered in the interpolation. Further analysis of the Variation Raster (Fig. 10) emphasizes that geodetic and ~~glaciologic~~glaciological mass balances do not only differ due to debris cover or other local effects. More precisely, it is evident that the deviations depend on the altitude. Thus, in the lower ~~reaches~~parts of the glacier, the geodetic mass balance is less negative than the glaciological mass ~~balances~~balance. For higher altitudes, the geodetic mass balance _is_ more negative than

370 the glaciologically derived ~~ones~~one. This pattern is usually attributed to the ice dynamic component of elevation change contained in the geodetic differences (submergence and emergence of ice and firn). Additionally, Fig. 9 clearly shows that comparing the different observation periods, the bias between both methods becomes larger within the accumulation areas.

15
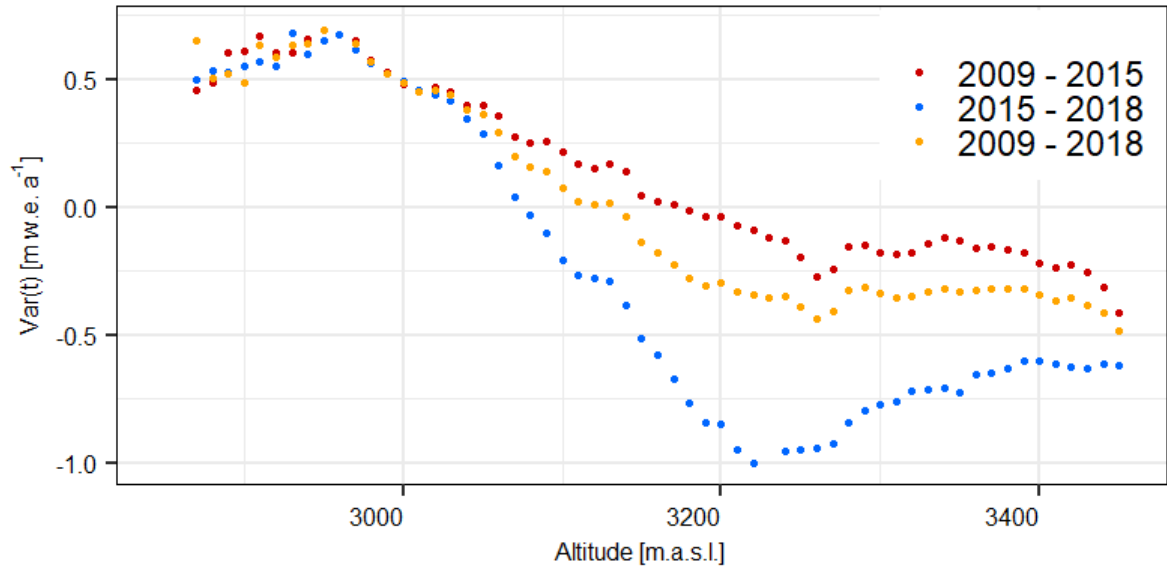
Figure 9: Methical variations between ~~corrected (Sect. 4.2.)~~<u>annual</u> **geodetic** <u>(corrected)</u> **and** ~~glaciologic~~<u>glaciological</u> **mass balances, depending on the altitude [m w.e. a⁻¹] for all periods t; Positive values are present where $B_{glac,t} < B_{geod,t}$, negative values are present for the opposite relation, see Eq. 7.**

Assuming all variations between geodetic and ~~glaciologic~~<u>glaciological</u> derived mass balances (Fig. 9) are caused by dynamic processes, the magnitude of emergence and submergence is computed using the Variation Raster and

380 Eq. 1 and 2. Between 2009 and 2018, the mean emergence (between 2900 m.a.s.l. and 3050 m.a.s.l.) is 0.55 ± 0.25 m w.e. a⁻¹, with a most positive value being 0.7 ± 0.25 m w.e. a⁻¹. Submergence occurs at altitudes higher than 3150 m.a.s.l. and results in a mean of $- 0.31 \pm 0.25$ m w.e. a⁻¹, with the most negative value being -0.48 ± 0.25 m w.e. a⁻¹ (Figure 10 and Table 3). For a glacier in balance, the change between submergence and emergence regions occurs close to the equilibrium line. However, the mean ELA of the Vernagtferner lies at 3237 m.a.s.l. for the

385 period 2009-2018 and thus roughly 150 m higher than the switch between apparent emergence and submergence. When comparing the five different accumulation basins of the Vernagtferner the derived submergence is more negative for higher basins with the largest offsets for the remaining true accumulation regions Hochvernagt and Taschachhochjoch (Figure 10 and Table 3).
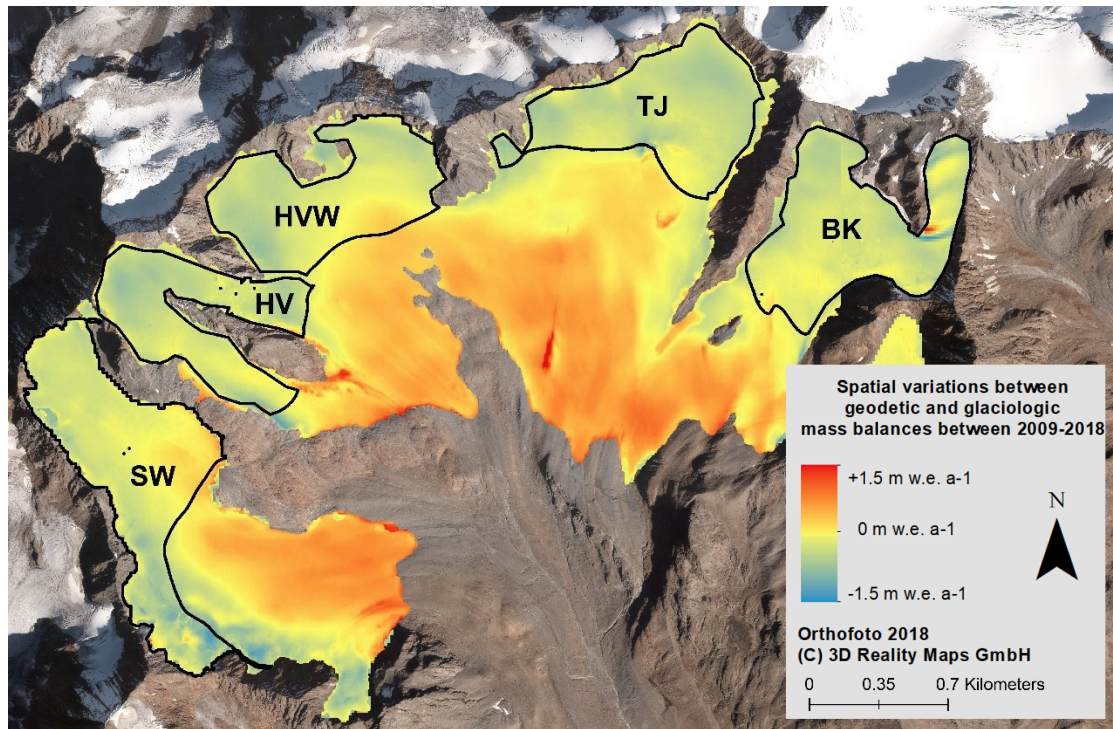
Figure 10: Top: Variation Raster 2009–2018: Spatial variations of the ~~corrected~~annual **geodetic (corrected) and** ~~glaciologie~~glaciological **mass balance data; Blue areas with negative variations represent areas where $B_{geod,t} < B_{glac,t}$. In red areas, the opposite relation is present (see Eq. 7). For regions that appear yellow, both methods present similar mass balances; Black outlines represent the different accumulation areas of the Vernagtferner.**

Table 3: Mean ~~variation and the respective area. Variation~~ **values of the** <u>Variation Raster 2009-2018 (Fig. 10) for the</u> **accumulation areas** ~~are given~~ **in m w.e. a^{-1},** ~~having an associated~~<u>interpreted as submergence; Associated</u> **error** ~~of~~<u>is</u> **± 0.25 m w.e a^{-1}** <u>for all submergence values</u>.

Accumulation Area		Mean submergence between 2009 and 2018 [m w.e. a^{-1}]	Area > 3150 m.a.s.l. [km²]
SW	Schwarzwand	- 0.26	0.69
HV	Hochvernagt	- 0.38	0.44
HVW	Hochvernagtwand	- 0.30	0.54
TJ	Taschachhochjoch	- 0.41	0.56
BK	Brochkogel	- 0.28	0.62
VN	**Vernagtferner (total)**	**- 0.32**	**2.85**

5.3 Other glaciers within the study site

The major advantage of geodetic mass balances compared to glaciological mass balances is that large areas can be investigated in great spatial detail. To highlight this benefit, we investigated the geodetic mass balance of all glaciers ~~in~~within the study area (Sect. 4.1.2). The ~~mean~~temporally uncorrected geodetic mass balance of all glaciers is -0.46 ± 0.06 m w.e. a^{-1} between 09/2009 and 08/2015, while it quadruples to -1.59 ± 0.21 m w.e. a^{-1} between 08/2015 and 09/2018. For the ~~whole~~aggregated period (09/2009–09/2018), the ~~mean~~uncorrected geodetic mass balance of all glaciers is -0.84 ± 0.11 m w.e. a^{-1}. It must be noted that ~~there was no~~the quadrupling of the geodetic mass balance is partly due to the temporal correction ~~applied for the acquisition times. Accordingly~~that

17

was not carried out. Thus, the mass balances do not refer to the glaciological year and cannot be compared with glaciological data.
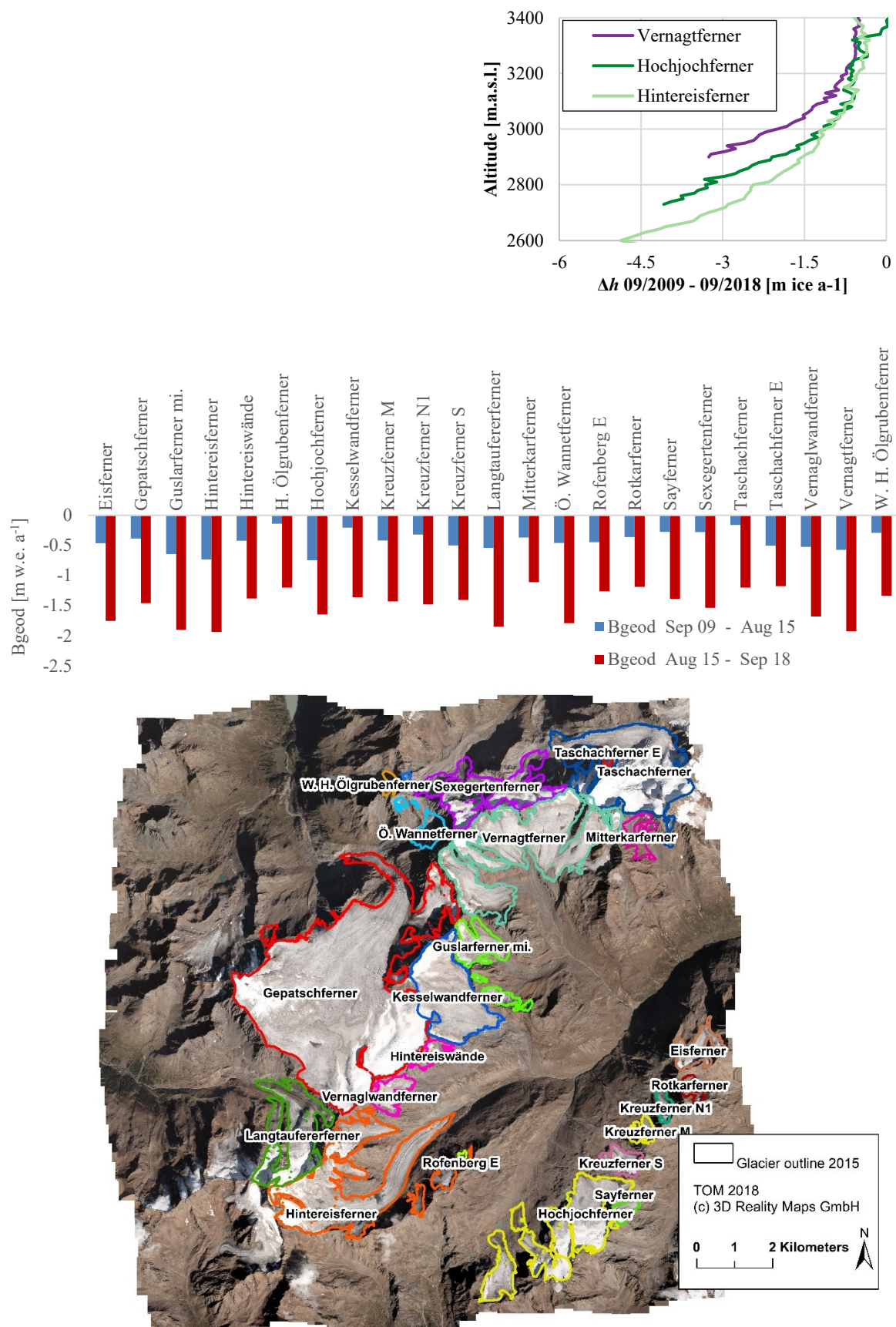
Figure : Annual height changes per altitude between 09/2009 and 09/2018 for the Vernagtferner compared to (i) all glaciers within the study area (top left) and (ii) to the Hochjochferner and Hintereisferner (top right); Comparison of geodetic mass balances of all glaciers within the study area for the two investigation periods (middle); glacier outlines of 2015 shown on TOM 2018 (bottom).

420

Name	$\Delta h_{\overline{K}}$ 09/2009 - 08/2015 [m]	$\Delta h_{\overline{K}}$ 08/2015 - 09/2018 [m]	$\Delta h_{\overline{K}}$ 09/2009 - 09/2018 [m]	B_{geod} 09/2009 - 08/2015 [m w.e. a⁻¹]	B_{geod} 08/2015 - 09/2018 [m w.e. a⁻¹]	B_{geod} 09/2009 - 09/2018 [m w.e. a⁻¹]	Area 2009 [km²]	Area 2015 [km²]	Area 2018 [km²]
Eisferner	-3.285	-6.199	-9.484	-0.465	-1.756	-0.896	0.836	0.773	0.628
Gepatschferner	-2.717	-5.149	-7.866	-0.385	-1.459	-0.743	18.951	18.775	18.589
Guslarferner mi.	-4.535	f-6.709	-11.243	-0.642	-1.901	-1.062	1.556	1.415	1.268
Hintereisferner	-5.175	-6.850	-12.025	-0.733	-1.941	-1.136	7.127	6.440	6.101
Hintereiswände	-2.977	-4.879	-7.856	-0.422	-1.382	-0.742	0.414	0.414	0.338
H. Ölgrubenferner	-0.999	-4.234	-5.232	-0.141	-1.200	-0.494	0.058	0.058	0.053
Hochjochferner	-5.261	-5.813	-11.075	-0.745	-1.647	-1.046	4.901	4.340	3.841
Kesselwandferner	-1.443	-4.806	-6.249	-0.204	-1.362	-0.590	3.697	3.597	3.563
Kreuzferner M	-2.967	-5.050	-8.017	-0.420	-1.431	-0.757	0.343	0.329	0.180
Kreuzferner N1	-2.252	-5.231	-7.483	-0.319	-1.482	-0.707	0.273	0.252	0.205
Kreuzferner S	-3.534	-4.965	-8.499	-0.501	-1.407	-0.803	0.559	0.531	0.456
Langtaufererferner	-3.836	-6.524	-10.360	-0.543	-1.849	-0.978	3.069	3.043	2.886
Mitterkar Ferner	-2.612	-3.930	-6.542	-0.370	-1.113	-0.618	0.536	0.536	0.515
Ö. Wannetferner	-3.249	-6.332	-9.581	-0.460	-1.794	-0.905	0.582	0.582	0.419
Rofenberg E	-3.154	-4.463	-7.616	-0.447	-1.264	-0.719	0.089	0.085	0.067
Rotkarferner	-2.552	-4.201	-6.753	-0.362	-1.190	-0.638	0.224	0.224	0.108
Sayferner	-1.949	-4.909	-6.858	-0.276	-1.391	-0.648	0.270	0.270	0.252
Sexegertenferner	-1.962	-5.429	-7.391	-0.278	-1.538	-0.698	2.980	2.905	2.462
Taschachferner	-1.143	-4.241	-5.384	-0.162	-1.202	-0.508	5.818	5.779	5.302
Taschachferner E.	-3.570	-4.153	-7.723	-0.506	-1.177	-0.729	0.049	0.049	0.049
Vernaglwandferner	-3.718	-5.941	-9.659	-0.527	-1.683	-0.912	0.745	0.700	0.576
Vernagtferner	-4.048	-6.802	-10.849	-0.573	-1.927	-1.025	7.327	7.015	6.096
W.H. Ölgrubenferner	-2.068	-4.724	-6.792	-0.293	-1.339	-0.641	0.143	0.143	0.128

If a time correction is assumed to have a similar influence on the annual mass balances of other glaciers as it had for the Vernagtferner (-34 % for 09/2009-08/2015, +20 % for 08/2015–09/2018, and +1.2 % for 09/2009–09/2018, Fig. 8), the meanannual mass balances of all glaciers can be estimated. Accordingly, the mean annual glacier mass

425 balance of all glaciers within the study area would be -0.61 ± 0.07 m w.e. a⁻¹ (2009-2015), -1.25 ± 0.14 m w.e. a⁻¹ (2015-2018) and -0.83 ± 0.1 m w.e. a⁻¹ (2009-2018). Thus, theBased on this assumption, annual geodetic mass balances would have doubled between the two periods 2009-2015 and 2015-2018 and the annual geodetic mass balance of the Vernagtferner for the same periods is 25 %, 21 %, and 22 % more negative than the mean of all glaciers (Fig. 8).

430 The remaining error due to the horizontal shift of the 2009 DOM (Sect. 5.1.2) is negligible for these general considerations but must be taken into account when working with individual mass balances (Table 4, Fig. 11).

Table 4: Surface changes [m] and geodetic mass balances [m w.e. a⁻¹] of all glaciers within the study area. Geodetic mass balances were derived by using a fixed density factor (Sect. 4.1.2. and Figure 2); Values are temporally uncorrected and thus do not match the glaciological year; Glaciers marked with (*) must be considered with additional caution for the periods 09/-2009-08/2015 and 09/2009-09/2018 due to their orientation. Related errors are higher than the error estimates presented in this manuscript (Sect. 5.1.2.)

435

Name	Δh_k 09/2009 - 08/2015 [m]	Δh_k 08/2015 - 09/2018 [m]	Δh_k 09/2009 - 09/2018 [m]	B_{geod} 09/2009 - 08/2015 [m w.e. a^{-1}]	B_{geod} 08/2015 - 09/2018 [m w.e. a^{-1}]	B_{geod} 09/2009 - 09/2018 [m w.e. a^{-1}]	Area 2009 [km²]	Area 2015 [km²]	Area 2018 [km²]
Eisferner	-3.29	-6.20	-9.48	-0.47	-1.76	-0.90	0.84	0.77	0.63
Gepatschferner	-2.72	-5.15	-7.87	-0.39	-1.46	-0.74	18.95	18.78	18.59
Guslarferner mi.	-4.54	-6.71	-11.24	-0.64	-1.90	-1.06	1.56	1.42	1.27
Hintereisferner	-5.18	-6.85	-12.03	-0.73	-1.94	-1.14	7.13	6.44	6.10
Hintereiswände	-2.98	-4.88	-7.86	-0.42	-1.38	-0.74	0.41	0.41	0.34
H. Ölgrubenferner	-1.00	-4.23	-5.23	-0.14	-1.20	-0.49	0.06	0.06	0.05
Hochjochferner	-5.26	-5.81	-11.08	-0.75	-1.65	-1.05	4.90	4.34	3.84
Kesselwandferner	-1.44	-4.81	-6.25	-0.20	-1.36	-0.59	3.70	3.60	3.56
Kreuzferner M (*)	-2.97	-5.05	-8.02	-0.42	-1.43	-0.76	0.34	0.33	0.18
Kreuzferner N1 (*)	-2.25	-5.23	-7.48	-0.32	-1.48	-0.71	0.27	0.25	0.21
Kreuzferner S (*)	-3.53	-4.97	-8.50	-0.50	-1.41	-0.80	0.56	0.53	0.46
Langtaufererferner	-3.84	-6.52	-10.36	-0.54	-1.85	-0.98	3.07	3.04	2.89
Mitterkar Ferner	-2.61	-3.93	-6.54	-0.37	-1.11	-0.62	0.54	0.54	0.52
Ö. Wannetferner	-3.25	-6.33	-9.58	-0.46	-1.79	-0.91	0.58	0.58	0.42
Rofenberg E (*)	-3.15	-4.46	-7.62	-0.45	-1.26	-0.72	0.09	0.09	0.07
Rotkarferner (*)	-2.55	-4.20	-6.75	-0.36	-1.19	-0.64	0.22	0.22	0.11
Sayferner (*)	-1.95	-4.91	-6.86	-0.28	-1.39	-0.65	0.27	0.27	0.25
Sexegertenferner	-1.96	-5.43	-7.39	-0.28	-1.54	-0.70	2.98	2.91	2.46
Taschachferner	-1.14	-4.24	-5.38	-0.16	-1.20	-0.51	5.82	5.78	5.30
Taschachferner E.	-3.57	-4.15	-7.72	-0.51	-1.18	-0.73	0.05	0.05	0.05
Vernaglwandferner	-3.72	-5.94	-9.66	-0.53	-1.68	-0.91	0.75	0.70	0.58
Vernagtferner	-4.05	-6.80	-10.85	-0.57	-1.93	-1.03	7.33	7.02	6.10
W.H. Ölgrubenferner	-2.07	-4.72	-6.79	-0.29	-1.34	-0.64	0.14	0.14	0.13
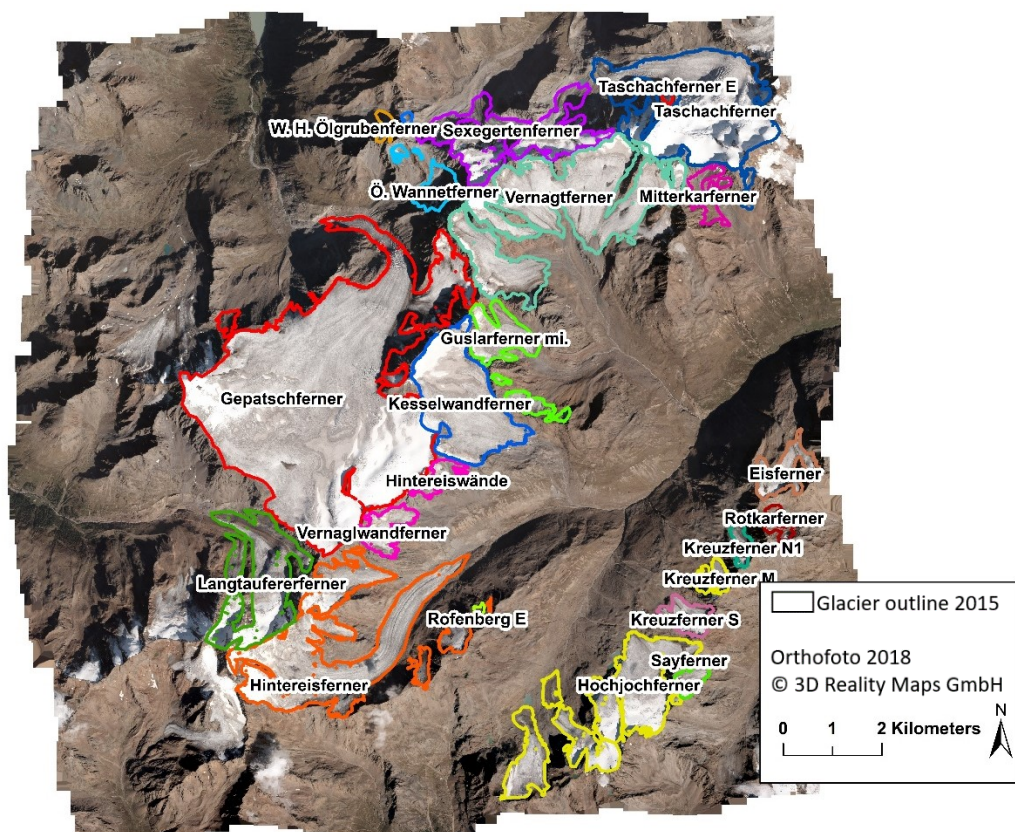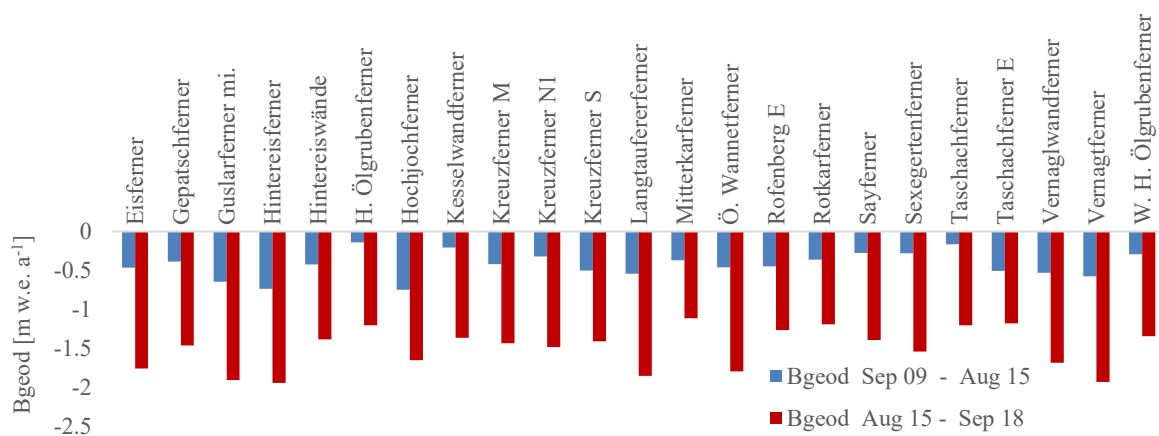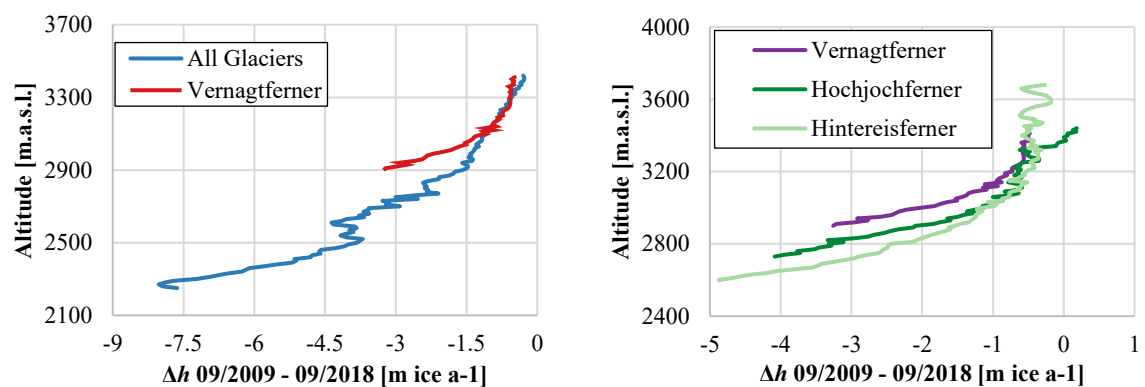
440

Figure 11

6   Discussion

This study investigated multitemporal changes in surface heights of selected glaciers in the Ötztal Alps with high

450   spatial resolution. We derived geodetic mass balances for 23 glaciers within our study area and found that glacier mass loss accelerated within the last decade. At the same time, the absolute surface height changes showed a maximum at low altitudes for all glaciers (Fig. 7). Peak volume loss occurs at higher altitudes, compared to the altitude where maximum surface height losses occur since the volume is directly linked to the area-height-distribution of a glacier. These findings correspond to general observations (i) for the Vernagtferner (BAdW, 2019;

455   Escher-Vetter, 2015) and (ii) for most of the glaciers in the Alps (~~Fischer et al., 2015b; Fischer et al., 2015a; Huss, 2012). Derived geodetic mass balances (Table 4) are well in accordance with the literature. For instance, the derived geodetic mass balance of the Hintereisferner (1.14 ± 0.02 m w.e. a⁻¹, Table 4) for the period 09/2009 – 09/2018 differs by only 8 % compared to the glaciologic mass balance of the same period (1.238 m w.e. a⁻¹ (WGMS, 2020)), measured by the Institute of Atmospheric and Cryospheric Sciences of the University in~~

460   ~~Innsbruck.~~Davaze et al., 2020; Fischer et al., 2015b; Fischer et al., 2015a; Huss, 2012).

We further evaluated the vertical surface height changes as a function of elevation (Fig. 7). Even though they cannot be directly compared to glaciologically derived vertical balance profiles, they illustrate the relation of height losses to altitude (Kaser et al., 2003; Pellikka and Rees, 2010). We found that the elevation changes of all glaciers within our study site (i) are on average less negative compared to the Vernagtferner, (ii) are correlated to the

465   altitude of the glacier tongue, and (iii) increased between 09/2009–08/2015 and 08/2015–09/2018 (Fig. 11). Besides glacier analysis, surface elevation changes caused by other processes (e.g. dead-ice bodies, debris movement) can be identified using high-resolution photogrammetric data. For instance, on the north-facing side of the valley, below the glacier tongue of Hintereisferner, existing surface elevation changes (Fig. 4), that can mostly be attributed to an existing dead ice body, were analyzed: Over an area of $27 * 10^4$ m², volume loss was

470   quantified to be ~~(5.7 ± 0,98) * 10⁶~~ $(1.3 \pm 0.22) * 10^6$ m³ for the period 2009 – 2018.

The error assessment ~~conducted reveals~~revealed the general high precision of ~~the~~ photogrammetric data with the SD of the vertical error not exceeding 0.42 m for all DSM differences (Fig. 6). The variation of the vertical error is normally distributed. ~~A~~ and semivariograms determined to assess the error for averaged values show a sill for all periods (further information on the method can be found in Rolstad et al. (2009)). However, a relation was

475   found for the vertical error regarding the aspect for the period 09/2009-08/2015 and 09/2009-09/2018, which is presumably based on a horizontal shift of the DSM 2009 (Sect. 4.1.1). ~~This~~Thus, assumptions made hereupon (Sect. 4.3.) are potentially less valid, meaning that the relation to the aspect can cause ~~a~~ larger error ~~than the value~~bars then we suggest~~, especially~~. Especially for glaciers with homogeneous ~~orientations~~orientation to the north or northwest, presented values must be considered with caution. However, only a few glaciers are affected

480   by this and are highlighted accordingly in this manuscript. By applying a full coregistration, following Nuth and Kääb (2011), this rotational error could have been addressed. ~~Nevertheless, the 95% confidence interval used in this study covers most of these variations (). Semivariograms determined to assess the error for averaged values~~

~~prove that this assumption is valid since semivariance approximates a clear sill (further information on the method can be found in Rolstad et al. (2009)).~~

485 We used the density assumption of Huss (2013) to convert height changes to water equivalent for all glaciers except for the Vernagtferner, that is repeatedly used for volume to mass conversions in other studies (~~e.g.~~ Andreassen et al., 2016; Belart et al., 2019~~). The~~). All DSM differences ~~09/2009–09/2018 and 09/2009–08/2015~~ fulfill the prerequisites for this density assumption (Huss, 2013). ~~This is not the case for~~However, the DSM difference 08/2015 – 09/2018 being a <u>rather short</u> period of only three years <u>just meets those requirements</u>.

490 Thus, the density assumption and the derived geodetic mass balances for this period must be considered with caution. For the Vernagtferner, we applied an altitude-related density function based on the known ELA. Since the density of the glacier volume lost is related to the ELA, our approach is more suitable for shorter time periods where the influence of annual meteorological conditions is increased, compared to the static density assumption provided by Huss (2013). For the Vernagtferner, ELA increased 61 m between our two study periods 2009 – 2015

495 and 2015 – 2018. This relatively small change in elevation changed the AAR of this glacier by about 15% and thus has an influence on the density of the volume lost during those periods that should not be neglected. The presented density function accounts for such changes of the AAR and thus allows a more detailed spatial comparison of the geodetic and ~~glaciologic~~glaciological mass balances. Since the ELA can be estimated from satellite imagery (Rabatel et al., 2005~~),~~), our method is transferable to other glaciers. We recommend, however,

500 adjusting the firn density values to the corresponding region. The presented altitude-related density function is easily applicable and needs low computational effort and therefore greatly complements other existing density conversion factors, that account for e.g. firn compaction processes, rely on classification methods or modelling (Pelto et al., 2019; Reeh, 2008).

<u>Derived geodetic mass balances (Table 4) are well in accordance with the literature. For instance, the derived</u>
505 <u>geodetic mass balance of the Hintereisferner (-1.14 ± 0.02 m w.e. a^{-1}, Table 4) for the period 09/2009 – 09/2018</u>
<u>differs by only 8 % compared to the glaciological mass balance of the same period (-1.24 m w.e. a^{-1} (WGMS,</u>
<u>2020)), measured by the Institute of Atmospheric and Cryospheric Sciences of the University in Innsbruck.</u>
<u>However, since geodetic surveys are not always possible at the end of the glaciological year, there are large</u>
<u>deviations (especially for the shorter periods 09/2009-08/2015 and 08/2015-09/2018) from the glaciological</u>
510 <u>periods and thus a direct comparison with glaciological mass balances is not possible. As a result, the mass</u>
<u>balances shown in Table 4 are influenced by the temporal offset, which causes parts of the observed increase in</u>
<u>mass balance magnitude. This must be considered for any further use.</u>

We developed a ~~robust~~ methodology to <u>account for this temporal offset thus to</u> adjust geodetic mass balances to the ~~acquisition time~~end of the ~~glaciologic measurements~~glaciological year (30th September). An additional UAV
515 survey was conducted, which allowed assessing vertical height changes during one month of the ablation period in 2018 (Fig. 3). Therefrom, a regression function (sigmoid) was determined to estimate surface changes relative to the elevation. We incorporated meteorological data from a nearby climate station by using a simple degree-day model for all relevant periods and elevation bins. Our regression function includes uncertainty for the accumulation areas since the UAV survey did not cover the entire glacier area. However, we showed that the presented workflow
520 provides good results as corrected <u>annual</u> geodetic mass balances agree well with glaciological mass balances (Fig. 8). Those results suggest that ~~the presented~~our method is ~~suitable~~suited for retrospective corrections of geodetic mass balances and can improve comparisons of geodetic with ~~glaciologic~~glaciological mass balances. However,

~~our~~the method will perform best if the AAR and area-height distribution remain similar between the period to be corrected and the period of the determined correction function. Thus, the retrospective correction is limited to a

525 few years only. The presented method complements other existing correction methods that rely, for instance, on field data, available for only a few glaciers, or DDF-models that do not have spatially explicit output (Belart et al., 2019; Fischer, 2011). ~~For transferability to other glaciers~~It must be noted that our method was only tested on the Vernagtferner for a limited number of observation periods and thus further testing is required to assess its robustness and transferability to other glaciers and periods. Therefore, individual correction functions must be

530 determined for each glacier individually, as these are directly related to glacier-specific slope gradients, orientation, the height of the glacier tongue, and area-height distributions (Fig. 11). To determine such individual correction functions, temperature information (for the correction period as well as all periods to which the correction is applied) and an additional geodetic survey is needed to estimate the surface elevation changes during the correction period. The length of the correction period was one month within this study, however we do not

535 expect poorer results if varying this period by 1-2 weeks. The required geodetic survey is neither limited to a platform, nor to a sensor. Thus, all geodetic survey configurations that allow the determination of geodetic glacier mass balances from DSM differences are suited for deriving the presented correction function. We used a dedicated photogrammetry-based UAV survey, flexible and low-cost, that enabled a correction with high spatial resolution. Comparing the corrected geodetic with interpolated ~~glaciologic~~glaciological mass balance rasters revealed local

540 deviations (Fig. 10). They mainly occur in crevassed and debris-covered areas and thus agree with findings of other studies (Fischer, 2011; Pellikka and Rees, 2010). They originate in the lack of ~~glaciologic~~glaciological ablation stakes that are not located in such areas, and thus the ~~glaciologic~~glaciological method interpolates within those regions. For crevassed areas, the deviations found at the Vernagtferner are negligible. Regarding the influence of debris cover for the period 2009 - 2018, we found that ~~glaciologic~~glaciological mass balance would

545 be ~~7.7~~2 % less negative if such regions would be considered within interpolation. Debris-~~ ~~cover might play an increasing role when debris-covered glacier areas increase due to further glacier decline (Scherler et al., 2018). This increases the need to conduct geodetic observations in addition to glaciological measurements because point measurements on debris-covered parts are not always representative.

Surprisingly, the differences between geodetic and glaciological volume change in the accumulation areas do not

550 reveal large spatial deviations, even though the glaciological results rely on very sparse in-situ data. This demonstrates that the long-term accumulation conditions at Vernagtferner, which are known from former detailed investigations (Mayer et al., 2013a; Mayer et al., 2013b), are spatially relatively stable and can be used for scaling the point measurements. However, this comparison of geodetic and glaciological results in the accumulation region has the potential to improve the representation of spatial variability across these areas.

555 The deviations between the geodetic and ~~glaciologic~~glaciological mass balances also showed a clear dependency on the elevation (Fig. 9) for all periods. These deviations are constant for the ablation areas for all periods but vary for the accumulation areas by a factor of three. We assumed that internal and basal melting is negligible, and the influence of temporal snowpack differences is small due to the long period of investigation and the rather small ratio of accumulation area. We thus interpret the variations as the large-scale dynamic processes submergence and

560 emergence. They become quantifiable when looking at the mean variations per altitude of both methods (Fig. 9 and 10). It is noticeable that the observed switch between emergence and submergence (Fig. 9) is about 100 m below the ELA of the Vernagtferner for the respective period 2009-2018 (BAdW, 2019) and roughly 200 m below

25

the ELA for the period 2015-2018. While the ELA increased between the two periods (2009-2015 vs. 2015-2018) by 61 m, the change from submergence to emergence decreased by about 130 m. The reasons for this development

565   are unknown but might indicate a further deviation from balanced conditions during recent years. The derived submergence must be considered with high caution since it is neither validated with field measurements nor model results. Presented submergence values are also based on (i) our applied correction with sparse data for the accumulation region, (ii) on the interpolation of a few ~~glaciologie~~glaciological stake readings, and (iii) our assumption that internal and basal processes are negligible. Those values (Table 3) are thus error-prone and should

570   only be referred to as a rough estimation. However, they show differences between the individual accumulation areas, which support glaciological observations (Lambrecht et al., 2011; Mayer et al., 2013b).

Future aerial image acquisitions aiming at calculating glacier mass balances must be as close as possible to each other (same date within the year) and preferably at the end of the ablation season. Ideally, these acquisitions are taken close to the standard glaciological mass balance data of 30th September to allow a direct comparison with

575   available field information. It should be ensured that the survey covers the entire surface of the glacier~~.~~ and that derived DOMs are fully coregistered. Since aerial image surveys require cloud-free weather, it will not always be possible to acquire the images on this exact date. This paper presented a ~~robust~~ method to account for the resulting differences in acquisition dates and to project geodetic mass balances to full ~~glaciologie~~glaciological periods.

For future research in the presented field, we see great potential in reanalyzing glacier mass balances using existing

580   aerial imagery. Since the late 2000s, European state surveying agencies have been carrying out cadastral surveys every two to four years with digital sensors with forward overlap of 80% and side overlap of 40-60 %, thus creating an immense multitemporal database of aerial imagery suitable for such purposes. The scientific and commercial consideration of those imageries would allow a three-dimensional reconstruction, mapping, and multitemporal analysis of vast areas in the Alps with a resolution in the order of decimetres.

585

26

7   Conclusion

This study demonstrates the potential of aerial images and the resulting DSM's for analyzing glacier retreat in great spatial and temporal detail. For all 23 glaciers within the study area, geodetic mass balances were derived with 0.2 m spatial resolution. It was shown that glacier retreat does not only take place in low altitudes, but that even

590   high accumulation basins are meanwhile affected due to non-compensated ice flow. The elevation of the highest glacier height changes and the amount of maximum volume loss increased within our observation period (2009-2018). In the future, if all aerial surveys that are available for large parts of the Alps were used, the majority of all alpine glaciers could be analyzed with the presented method. The spatial resolution of the respective analysis would be significantly better than in other recent satellite-based studies. We compared the photogrammetric results

595   with glaciological in-situ measurements of the Vernagtferner. An altitude-related density assumption was used to account for the rise of the ELA and to increase the spatial detail of the comparison with the ~~glaciologie~~glaciological data. Geodetic mass balance periods were adjusted to the ~~glaciologie~~glaciological survey dates by ~~applying~~using an additional UAV survey, combined with a simple degree-day model. This correction as well as our density function ~~allow~~allowed a spatially explicit, retrospective determination and correction of geodetic mass balances

600   and is transferable to other glaciers. The results show that the glaciological method can be greatly complemented with photogrammetric analyses, increasing the accuracy of the glaciological mass balance series, revealing regions of anomalous mass balance conditions, and allowing estimates of the imbalance between mass balance and ice dynamics.

27

8   References

Abermann, J., Lambrecht, A., Fischer, A. and Kuhn, M.: Quantifying changes and trends in glacier area and volume in the Austrian Ötztal Alps (1969-1997-2006), The Cryosphere, 3, 205–215, https://doi.org/10.5194/tc-3-205-2009, 2009.

Andreassen, L. M., Elvehøy, H., Kjøllmoen, B. and Engeset, R. V.: Reanalysis of long-term series of glaciological and geodetic mass balance for 10 Norwegian glaciers, The Cryosphere, 10, 535–552, https://doi.org/10.5194/tc-10-535-2016, 2016.

Auer, I., Böhm, R., Jurkovic, A., Lipa, W., Orlik, A., Potzmann, R., Schöner, W., Ungersböck, M., Matulla, C., Briffa, K., Jones, P., Efthymiadis, D., Brunetti, M., Nanni, T., Maugeri, M., Mercalli, L., Mestre, O., Moisselin, J.-M., Begert, M., Müller-Westermeier, G., Kveton, V., Bochnicek, O., Stastny, P., Lapin, M., Szalai, S., Szentimrey, T., Cegnar, T., Dolinar, M., Gajic-Capka, M., Zaninovic, K., Majstorovic, Z. and Nieplova, E.: HISTALP—historical instrumental climatological surface time series of the Greater Alpine Region, Int. J. Climatol., 27, 17–46, https://doi.org/10.1002/joc.1377, 2007.

BAdW: Mass balance of the Vernagtferner, AT: https://geo.badw.de/vernagtferner-digital/massenbilanz.html, last access: 19 July 2019.

Baltsavias, E. P., Favey, E., Bauder, A., Bosch, H. and Pateraki, M.: Digital Surface Modelling by Airborne Laser Scanning and Digital Photogrammetry for Glacier Monitoring, The Photogrammetric Record, 17, 243–273, https://doi.org/10.1111/0031-868X.00182, 2001.

Bamber, J. L. and Rivera, A.: A review of remote sensing methods for glacier mass balance determination, Global and Planetary Change, 59, 138–148, https://doi.org/10.1016/j.gloplacha.2006.11.031, 2007.

Belart, J. M. C., Magnússon, E., Berthier, E., Pálsson, F., Adalgeirsdottir, G. and Jóhannesson, T.: The geodetic mass balance of Eyjafjallajökull ice cap for 1945–2014: processing guidelines and relation to climate, 0022-1430, https://doi.org/10.1017/jog.2019.16, 2019.

Beniston, M., Farinotti, D., Stoffel, M., Andreassen, L. M., Coppola, E., Eckert, N., Fantini, A., Giacona, F., Hauck, C., Huss, M., Huwald, H., Lehning, M., López-Moreno, J.-I., Magnusson, J., Marty, C., Morán-Tejéda, E., Morin, S., Naaim, M., Provenzale, A., Rabatel, A., Six, D., Stötter, J., Strasser, U., Terzago, S. and Vincent, C.: The European mountain cryosphere: a review of its current state, trends, and future challenges, The Cryosphere, 12, 759–794, https://doi.org/10.5194/tc-12-759-2018, 2018.

Braithwaite, R. J. and Zhang, Y.: Sensitivity of mass balance of five Swiss glaciers to temperature changes assessed by tuning a degree-day model, Journal of Glaciology, 46, 7–14, https://doi.org/10.3189/172756500781833511, 2000.

Cogley, G.: Mass-balance terms revisited, Journal of Glaciology, 56, 997–1001, https://doi.org/10.3189/002214311796406040, 2010.

Cogley, G., Hock, R., Rasmussen, L. A., Arendt, A. A. and Zemp, M.: Glossary of glacier mass balance and related terms, 86, https://doi.org/10.5167/uzh-53475, 2011.

Davaze, L., Rabatel, A., Dufour, A., Hugonnet, R. and Arnaud, Y.: Region-Wide Annual Glacier Surface Mass Balance for the European Alps From 2000 to 2016, Front. Earth Sci., 8, 149, https://doi.org/10.3389/feart.2020.00149, 2020.

660 Escher-Vetter, H.: 400 Jahre Feldforschung am Vernagtferner (Ötztal, Österreich), Lozan, J. L.; Graßl, H.;
Kasang, D.; Notz, D.; Escher-Vetter, H. (5 editors) / Warnsignal Klima / Wissenschaftliche Auswertungen,
Hamburg, 299pp, ch. 4.7 (146-154), 2015.

Escher-Vetter, H., Kuhn, M. and Weber, M.: Four decades of winter mass balance of Vernagtferner and
Hintereisferner, Austria: methodology and results, Annals of Glaciology, 50, 87–95,
665 https://doi.org/10.3189/172756409787769672, 2009.

Fischer, A.: Comparison of direct and geodetic mass balances on a multi-annual time scale, The Cryosphere, 5,
107–124, https://doi.org/10.5194/tc-5-107-2011, 2011.

Fischer, A., Schneider, H., Merkel, G. and Sailer, R.: Comparison of direct and geodetic mass balances on an
annual time scale, 2011.

670 Fischer, A., Seiser, B., Stocker Waldhuber, M., Mitterer, C. and Abermann, J.: Tracing glacier changes in
Austria from the Little Ice Age to the present using a lidar-based high-resolution glacier inventory in Austria,
The Cryosphere, 9, 753–766, https://doi.org/10.5194/tc-9-753-2015, 2015a.

Fischer, M., Huss, M. and Hoelzle, M.: Surface elevation and mass changes of all Swiss glaciers 1980–2010,
The Cryosphere, 9, 525–540, https://doi.org/10.5194/tc-9-525-2015, 2015b.

675 Fliri, F.: Das Klima der Alpen im Raume von Tirol, Wagner, Innsbruck, 1975.

Fugazza, D., Scaioni, M., Corti, M., D'Agata, C., Azzoni, R. Sergio, Cernuschi, M., Smiraglia, C. and Diolaiuti,
G. Adele: Combination of UAV and terrestrial photogrammetry to assess rapid glacier evolution and map
glacier hazards, Nat. Hazards Earth Syst. Sci., 18, 1055–1071, https://doi.org/10.5194/nhess-18-1055-2018,
2018.

680 Gobiet, A., Kotlarski, S., Beniston, M., Heinrich, G., Rajczak, J. and Stoffel, M.: 21st century climate change in
the European Alps - a review, The Science of the total environment, 493, 1138–1151,
https://doi.org/10.1016/j.scitotenv.2013.07.050, 2014.

Gudmundsson, G. H. and Bauder, A.: Towards an Indirect Determination of the Mass-balance Distribution of
Glaciers using the Kinematic Boundary Condition, Geografiska Annaler A, 81, 575–583,
685 https://doi.org/10.1111/1468-0459.00085, 1999.

Hanzer, F., Förster, K., Nemec, J. and Strasser, U.: Projected cryospheric and hydrological impacts of 21st
century climate change in the Ötztal Alps (Austria) simulated using a physically based approach, Hydrology
and Earth System Sciences, 22, 1593-1614, https://doi.org/10.15488/3378, 2018.

Heipke, C.: Photogrammetrie und Fernerkundung, Springer, Berlin, Heidelberg, Germany, 2017.

690 Hirschmüller, H.: Semi-Global Matching. Motivation, Developments and Applications, available at:
https://elib.dlr.de/73119/1/180Hirschmueller.pdf, 2019.

Hock, R.: Temperature index melt modelling in mountain areas, Journal of Hydrology, 282, 104–115,
https://doi.org/10.1016/S0022-1694(03)00257-9, 2003.

Huss, M.: Extrapolating glacier mass balance to the mountain-range scale: the European Alps 1900–2100, The
695 Cryosphere, 6, 713–727, https://doi.org/10.5194/tc-6-713-2012, 2012.

Huss, M.: Density assumptions for converting geodetic glacier volume change to mass change, The Cryosphere,
7, 877–887, https://doi.org/10.5194/tc-7-877-2013, 2013.

Huss, M., Bauder, A. and Funk, M.: Homogenization of long-term mass-balance time series, Annals of
Glaciology, 50, 198–206, https://doi.org/10.3189/172756409787769627, 2009.

29

700   Jaenicke, J., Mayer, C., Scharrer, K., Münzer, U. and Gudmundsson, A.: The use of remote-sensing data for mass-balance studies at Mýrdalsjökull ice cap, Iceland, Journal of Glaciology, 52, 565–573, https://doi.org/10.3189/172756506781828340, 2006.

Kääb, A.: Remote sensing of mountain glaciers and permafrost creep., Physical Geography Series 48, 53, 266pp., https://doi.org/10.3189/172756507781833857, 2005.

705   Kargel, J. S., Bishop, M. P., Kääb, A. and Raup, B.: Global Land Ice Measurements from Space, Springer, Dordrecht, 2013.

Kaser, G., Fountain, A., Jansson, P., Heucke, E. and Knaus, M.: A manual for monitoring the mass balance of mountain glaciers, UNESCO, 137 pp., available at: https://globalcryospherewatch.org/bestpractices/docs/UNESCO_manual_glaciers_2003.pdf, 2003.

710   Klug, C., Bollmann, E., Galos, S. Peter, Nicholson, L., Prinz, R., Rieg, L., Sailer, R., Stötter, J. and Kaser, G.: Geodetic reanalysis of annual glaciological mass balances (2001–2011) of Hintereisferner, Austria, The Cryosphere, 12, 833–849, https://doi.org/10.5194/tc-12-833-2018, 2018.

Lambrecht, A., Mayer, C., Hagg, W., Popovnin, V., Rezepkin, A., Lomidze, N. and Svanadze, D.: A comparison of glacier melt on debris-covered glaciers in the northern and southern Caucasus, The Cryosphere, 5, 525–

715   538, https://doi.org/10.5194/tc-5-525-2011, 2011.

Legat, K., Moe, K., Poli, D. and Bollmann, E.: Exploring the potential of aerial photogrammetry for 3D modelling of high-alpine envirnoments, Int. Arch. Photogramm. Remote Sens. Spatial Inf. Sci., XL-3/W4, 97–103, https://doi.org/10.5194/isprs-archives-XL-3-W4-97-2016, 2016.

Magnússon, E., Muñoz-Cobo Belart, J., Pálsson, F., Ágústsson, H. and Crochet, P.: Geodetic mass balance

720   record with rigorous uncertainty estimates deduced from aerial photographs and lidar data – Case study from Drangajökull ice cap, NW Iceland, The Cryosphere, 10, 159–177, https://doi.org/10.5194/tc-10-159-2016, 2016.

Marty, C. and Meister, R.: Long-term snow and weather observations at Weissfluhjoch and its relation to other high-altitude observatories in the Alps, Theor Appl Climatol, 110, 573–583, https://doi.org/10.1007/s00704-

725   012-0584-3, 2012.

Mayer, C., Escher-Vetter, H. and Weber, M.: 46 Jahre glaziologische Massenbilanz des Vernagtferners, Zeitschrift für Gletscherkunde und Glazialgeologie, 45/46, 219–234, 2013a.

Mayer, C., Jaenicke, J., Lambrecht, A., Braun, L., Völksen, C., Minet, C. and Münzer, U.: Local surface mass-balance reconstruction from a tephra layer – a case study on the northern slope of Mýrdalsjökull, Iceland,

730   Journal of Glaciology, 63, 79–87, https://doi.org/10.1017/jog.2016.119, 2017.

Mayer, C., Lambrecht, A., Blumthaler, U. and Eisen, O.: Vermessung und Eisdynamik des Vernagtferners, Ötztaler Alpen, Zeitschrift für Gletscherkunde und Glazialgeologie, 45/46, 259–280, 2013b.

Nuth, C. and Kääb, A.: Co-registration and bias corrections of satellite elevation data sets for quantifying glacier thickness change, The Cryosphere, 5, 271–290, https://doi.org/10.5194/tc-5-271-2011, 2011.

735   Östrem, G.: Ice Melting under a Thin Layer of Moraine, and the Existence of Ice Cores in Moraine Ridges, Geografiska Annaler, 228–230, https://doi.org/10.1080/20014422.1959.11907953, 1959.

Pellikka, P. K. E. and Rees, W. G. (Eds.): Remote sensing of glaciers: techniques for topographic, spatial and thematic mapping of glaciers, Taylor & Francis, New York, USA, 2010.

Pelto, B. M., Menounos, B. and Marshall, S. J.: Multi-year evaluation of airborne geodetic surveys to estimate

740   seasonal mass balance, Columbia and Rocky Mountains, Canada, The Cryosphere, 13, 1709–1727, https://doi.org/10.5194/tc-13-1709-2019, 2019.

Rabatel, A., Dedieu, J.-P. and Vincent, C.: Using remote-sensing data to determine equilibrium-line altitude and mass-balance time series: validation on three French glaciers, 1994–2002, Journal of Glaciology, 51, 539–546, https://doi.org/10.3189/172756505781829106, 2005.

745   Reeh, N.: A nonsteady-state firn-densification model for the percolation zone of a glacier, J. Geophys. Res., 113, https://doi.org/10.1029/2007JF000746, 2008.

Rogora, M., Frate, L., Carranza, M. L., Freppaz, M., Stanisci, A., Bertani, I., Bottarin, R., Brambilla, A., Canullo, R., Carbognani, M., Cerrato, C., Chelli, S., Cremonese, E., Cutini, M., Di Musciano, M., Erschbamer, B., Godone, D., Iocchi, M., Isabellon, M., Magnani, A., Mazzola, L., Di Morra Cella, U., Pauli,

750   H., Petey, M., Petriccione, B., Porro, F., Psenner, R., Rossetti, G., Scotti, A., Sommaruga, R., Tappeiner, U., Theurillat, J.-P., Tomaselli, M., Viglietti, D., Viterbi, R., Vittoz, P., Winkler, M. and Matteucci, G.: Assessment of climate change effects on mountain ecosystems through a cross-site analysis in the Alps and Apennines, Science of The Total Environment, 624, 1429–1442, https://doi.org/10.1016/j.scitotenv.2017.12.155, 2018.

755   Rolstad, C., Haug, T. and Denby, B.: Spatially integrated geodetic glacier mass balance and its uncertainty based on geostatistical analysis: application to the western Svartisen ice cap, Norway, J. Glaciol., 55, 666–680, https://doi.org/10.3189/002214309789470950, 2009.

Rossini, M., Di Mauro, B., Garzonio, R., Baccolo, G., Cavallini, G., Mattavelli, M., Amicis, M. de and Colombo, R.: Rapid melting dynamics of an alpine glacier with repeated UAV photogrammetry,

760   Geomorphology, 304, 159–172, https://doi.org/10.1016/j.geomorph.2017.12.039, 2018.

Scherler, D., Wulf, H. and Gorelick, N.: Global Assessment of Supraglacial Debris-Cover Extents, Geophys. Res. Lett., 45, 798–805, https://doi.org/10.1029/2018GL080158, 2018.

Sommer, C., Malz, P., Seehaus, T. C., Lippl, S., Zemp, M. and Braun, M.: Rapid glacier retreat and downwasting throughout the European Alps in the early 21 st century, Nat Commun, 11, 1–10,

765   https://doi.org/10.1038/s41467-020-16818-0, 2020.

Vargo, L. J., Anderson, B. M., Horgan, H. J., Mackintosh, A. N., Lorrey, A. M. and Thornton, M.: Using structure from motion photogrammetry to measure past glacier changes from historic aerial photographs, Journal of Glaciology, 63, 1105–1118, https://doi.org/10.1017/jog.2017.79, 2017.

WGMS: Global Glacier Change Bulletin, available at: https://wgms.ch/products_ref_glaciers/hintereisferner-

770   alps/, 2020.

Zekollari, H., Huss, M. and Farinotti, D.: Modelling the future evolution of glaciers in the European Alps under the EURO-CORDEX RCM ensemble, The Cryosphere, 13, 1125–1146, https://doi.org/10.5194/tc-13-1125-2019, 2019.

Zemp, M., Thibert, E., Huss, M., Stumm, D., Rolstad Denby, C., Nuth, C., Nussbaumer, S. U., Moholdt, G.,

775   Mercer, A., Mayer, C., Joerg, P. C., Jansson, P., Hynek, B., Fischer, A., Escher-Vetter, H., Elvehøy, H. and Andreassen, L. M.: Reanalysing glacier mass balance measurement series, The Cryosphere, 7, 1227–1245, https://doi.org/10.5194/tc-7-1227-2013, 2013.